Lithium Niobate Meta-Optics

Anna Fedotova[1,2]*, Luca Carletti[3]*, Attilio Zilli[4], Frank Setzpfandt[2,5], Isabelle Staude[1,2], Andrea Toma[6], Marco Finazzi[4], Costantino De Angelis[3], Thomas Pertsch[2,5], Dragomir N. Neshev[7]†, and Michele Celebrano[4]†

[1] Friedrich Schiller University, Institute of Solid State Physics – Jena, Germany

[2] Friedrich Schiller University, Institute of Applied Physics, Abbe Center of Photonics – Jena, Germany

[3] University of Brescia, Department of Information Engineering and INO-CNR – Brescia, Italy

[4] Politecnico di Milano, Department of Physics – Milano, Italy

[5] Fraunhofer Institute for Applied Optics and Precision Engineering – Jena, Germany

[6] Istituto Italiano di Tecnologia – Genova, Italy

[7] ARC Centre of Excellence for Transformative Meta-Optical Systems (TMOS), Research School of Physics, Australian National University – Canberra ACT 2601, Australia

†Corresponding authors: dragomir.neshev@anu.edu.au, michele.celebrano@polimi.it

Abstract

The rapid development of optical metasurfaces—2D ensembles of engineered nanostructures—is presently underpinning a steady drive towards the miniaturization of many optical functionalities and devices. The list of material platforms for optical metasurfaces is rapidly expanding as, over the past few years, we have witnessed a surge in establishing meta-optical elements from high-index, highly transparent materials with strong nonlinear and electro-optic properties. In particular, crystalline lithium niobate ($LiNbO_3$), already a prime material for integrated photonics, has shown great promise for novel meta-optical components, thanks to its large electro-optical coefficient and second-order nonlinear response, and its broad transparency window ranging from the visible to the mid-infrared. Recent advances in nanofabrication technology have indeed marked a new milestone in the miniaturization of $LiNbO_3$ platforms, hence enabling the first demonstrations of $LiNbO_3$-based metasurfaces**.** These seminal works set a steppingstone toward the realization of ultra-thin monolithic nonlinear light sources, efficient quantum sources of correlated photon pairs, as well as electro-optical modulators. Here, we review these recent advances by providing a perspective on their potential applications and examining the possible setbacks and limitations of these emerging technologies.

1. Introduction

In the last decade, the field of meta-optics received a major boost, driven by the urge to realize ultra-compact photonic devices to shape and manipulate optical electromagnetic radiation.[1–8] The prefix 'meta', which means 'after' in the Greek language but is currently employed mostly with the meaning of 'beyond' in science and technology, epitomizes the mission of this research field: *i.e.,* pushing the capabilities and the integration of optical devices beyond that of conventional optics (*e.g.*, lenses, mirrors, filters, nonlinear crystals). The key enabling platforms at its core are optical metasurfaces, namely sub-micrometer thick devices based on engineered ensembles of electromagnetically coupled nanostructures (*i.e.* meta-atoms), which promise to complement and enrich the set of tools already available in optics and photonics.[2, 4–8] This intriguing opportunity is underpinned by the possibility to vastly tailor the optical properties of metasurfaces through the combined design of the individual meta-atoms and their ensemble disposition. In particular, optical metasurfaces can be engineered to simultaneously feature a variety of fundamental optical functionalities, such as polarization and wavefront control in a single ultra-thin device.[3, 8, 9] This is very appealing for photonic applications that require a high degree of integration, such as ultra-compact laser cavities (*e.g.*, vertical cavity surface-emitting laser), and can be applied even to waveguides.[10] Given their two-dimensional character, metasurfaces can also be stacked as multiple serial elements to attain more flexibility or add further functionalities.[7] The broad range of possibilities of this fascinating research topic has drawn the attention of the photonics community in the last couple of decades. Thus far, this revolution has mainly concerned refractive elements capable of manipulating the light wavefront by molding the spatial and temporal phase of the propagating beam.[1–8]

The development of nonlinear and tunable meta-optics, that is, realizing meta-devices capable of processing light beyond the linear refractive and diffractive regimes, has recently experienced a significant thrust, triggered by the tantalizing promises it holds, [11–13] yet it still remains largely unexplored. The main aim of these fields is to provide metasurfaces featuring additional functionalities, such as nonlinear light conversion, generation of entangled photon pairs, and dynamic light modulation (typically via electro-optic

effect). The typical materials of choice for such applications in photonic technology are semiconductors, such as silicon (Si), gallium arsenide (GaAs), or gallium phosphide (GaP); and ionic crystals, such as lithium niobate ($LiNbO_3$), beta barium borate (BBO), or potassium dihydrogen phosphate (KDP).[14] In particular, the extensive use of the latter ones is motivated by their sizable nonlinear optical coefficients as well as a broad transparency window that includes the visible spectrum. This allows these materials to withstand the high irradiance required to achieve a strong light–matter interaction. Moreover, the employment of long propagation lengths further compensates for the intrinsic weakness of the underlying processes. In addition, to further boost the light–matter interaction in nonlinear optics, phase-matching condition and crystal poling are exploited to optimize the overlap between the interacting fields.[14] The fundamental hindrance to overcome in tunable and nonlinear meta-optics is the dramatic reduction of light–matter interactions caused by the intrinsic down-sizing of the interaction volume. Indeed, optical metasurfaces are open photonic systems with sub-wavelength thicknesses, which makes their exploitation for this purpose extremely challenging. While the lack of phase matching in meta-optics undoubtedly decreases the efficiency of nonlinear processes, on the other hand it lifts the constraints on momentum, therefore enabling broadband nonlinear light conversion, as recently demonstrated in 2D materials.[15] Yet, to obtain efficient electro-optical modulation and nonlinear optical processes in meta-optics, alternative approaches must be devised to enhance the light–matter interaction over subwavelength distances. Plasmonic-based (*i.e.* metallic) metasurfaces were the first platforms proposed to tackle these challenges in nonlinear meta-optics, because of their ability to localize extremely intense fields at sub-wavelength scales.[2, 11, 12, 16] Still, the utmost drawback of these platforms lies in the large dissipative losses of metals, which limit the optical powers one can employ and, hence, the overall efficiency of the underlying processes.

The advances in state-of-the-art nanofabrication of CMOS-compatible platforms guided the recent development of semiconductor-based platforms for meta-optics.[17, 18, 19] To date, semiconducting metasurfaces have been successfully applied to nonlinear light conversion, light-by-light modulation, and

dynamic light steering. In particular, group IV semiconductors have been used for third-harmonic generation (THG), [20–22] whereas III−V semiconducting alloys have been employed for second-harmonic generation (SHG).[23–26] Nonetheless, because of their relatively narrow bandgaps with absorption onsets in the near-infrared (NIR) wavelength range, most of these platforms limit the development of low-loss nonlinear meta-optics, at least in the crucial visible region of the electromagnetic spectrum. The meta-optics components therefore need to incorporate highly transparent, high-index, functional materials, which have driven the quest for developing new material platforms, such as nanostructured ferroelectrics.

$LiNbO_3$ is widely-employed in integrated photonics,[27–29] thanks to its extremely wide transparency window (350–4500 nm) and unique nonlinear and electro-optical properties. Yet, due to the challenging fabrication of sub-micron features in this material, only very recently the application of $LiNbO_3$ to meta-optics has been theoretically[29–31] and experimentally[32–38] investigated. These preliminary studies have already

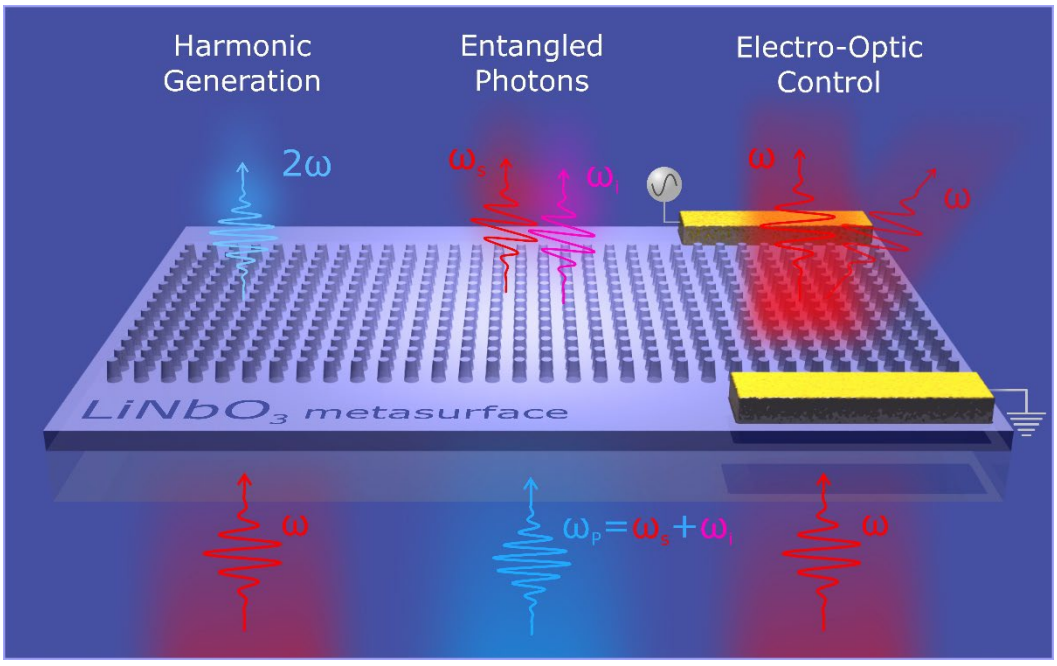

Figure 1. Examples of $LiNbO_3$ metasurfaces to nonlinear and electro-optics applications. (left) Frequency up-conversion via second-harmonic generation. (middle) Creation of entangled and correlated photon pairs via spontaneous parametric down-conversion. (right) Electrically reconfigurable metasurfaces for electro-optical beam modulation.

highlighted the potential of $LiNbO_3$ metasurfaces with reproducible nanometer-size features for nonlinear and tunable meta-optics in the NIR and visible range, as schematically depicted in Figure 1.

Being a non-centrosymmetric material, in $LiNbO_3$ the largest nonlinear and electro-optical effects are governed by the second-order susceptibility tensor $\chi^{(2)}$ (or the contracted nonlinear tensor $d = \frac{1}{2}\chi^{(2)}$, when Kleinman symmetry holds), which allows wave mixing processes between three distinct fields.[39] In addition, the trigonal crystal structure of $LiNbO_3$ with $3m = C_{3v}$ symmetry leads to nonvanishing values of the diagonal coefficients of the $\chi^{(2)}$ tensor, with the d_{33} component (associated with the *c*-axis) being the dominant one.[39,40] This is a particularly appealing property for nonlinear and electro-optics applications since it fosters the interaction of electric fields with the same polarization. This could be beneficial for realizing sources of entangled photons having identical polarization states via spontaneous parametric down-conversion (SPDC) in a metasurface (see Figure 1-middle).[41, 42] The possibility to cut the material along a cleavage plane of choice, hence defining a specific orientation of the crystalline axes, provides a further degree of freedom to engineer nonlinear optical processes in $LiNbO_3$-based platforms.

In the following we review the emerging field of $LiNbO_3$-based meta-optics, focusing on its key advantages and the perspectives that it can bring about in the medium to long term. We critically examine some fundamental challenges that need to be tackled in view of a full deployment of this technology. In Section 2 we present the optical properties of $LiNbO_3$, and in Section 3 we survey the approaches available for the nanofabrication of $LiNbO_3$ nanostructures and metasurfaces, as well as discuss future directions in material engineering and nanofabrication technologies for this material. In Section 4 we focus on the recent advances in the realization of $LiNbO_3$ metasurfaces for nonlinear and electro-optical light management. We cover the state-of-the-art in frequency doubling (Figure 1-left), photon-pair generation (Figure 1–middle), and electro-optical modulation (Figure 1–right).

2. Optical properties of $LiNbO_3$

$LiNbO_3$ is a dielectric uniaxial crystal, transparent over a broad wavelength range spanning from 350 nm in the ultra-violet (UV) to 4500 nm in the mid-infrared (MIR). Being a uniaxial crystal, $LiNbO_3$ is birefringent, thus enabling polarization control and manipulation. The birefringence of the material stems from the polar nature of its crystalline lattice, which also entails many peculiar functionalities like ferroelectricity, pyroelectricity and piezoelectricity, *i.e.*, the possibility of modifying the optical properties via external stimuli such as electric fields, temperature, and pressure, respectively.

Material	Refractive index (*n*) at λ = 1550 nm	Transparency window (μm)	Largest nonlinear coefficient (pm/V) / susceptibility (m^2/V^2)	Electro-optics coefficient (pm/V)
Non-centrosymmetric materials				
lithium niobate ($LiNbO_3$)	2.2	0.35 – 4.5	$d_{33} \approx 21$ [43] (5) $d_{33} \approx 27$ [39] (6)	$r_{33} \approx 31$ $r_{42} \approx 28$ [44, 45]
(aluminum) gallium arsenide ((Al)GaAs)	3.5	(0.7)[(1)] 0.9 – 18	$d_{36} \approx 170$ [46] (1) (6)	$r_{41} \approx 1.5$ [47] (5)
gallium phosphide (GaP)	3	0.45 – 14	$d_{36} \approx 70$ [46] (6)	$r_{41} \approx -1$ [48] (4)
gallium nitride (GaN)	2.3	0.37 – 7	$d_{33} \approx 10$ [49] (6)	$r_{33} \approx 1.9$ [50] (4)
barium titanate ($BaTiO_3$)	2.3	0.36 – 9	$d_{15} \approx 17$ [51, 52] (6)	$r_{33} \approx 340$ $r_{42} \approx 1000$ [53] (6)
halide perovskites	1.9	> 0.4 [(2)]	$d_{\text{eff}} \approx 1 \div 14$ [54] (3)	$r_{33} \approx 1.4$ [55] (6)
Centrosymmetric materials				
germanium (Ge)	4.2	1.8 – 20	$\chi^{(3)} \approx 5.6 \times 10^{-19}$ [14]	
silicon (Si)	3.5	1 – 8	$\chi^{(3)} \approx 2.8 \times 10^{-18}$ [14]	

Table 1. Linear and nonlinear optical properties of $LiNbO_3$ compared to other widely used dielectric materials. Notes: (1) For aluminum concentration of about 20%. (2) The bandgap varies widely but, for most perovskites, it is above 700 nm. (3) Nonlinear coefficients strongly depend on the perovskite constituents. Values reported at (4) 633 nm, (5) 1060 nm, (6) 1550 nm.

However, the most relevant feature of $LiNbO_3$ for nonlinear optics applications is its relatively high second-order susceptibility, enabled by the broken inversion symmetry of the crystalline lattice—one of the highest among the ionic crystals in the technologically-relevant telecom wavelength range (*i.e.,* around 1550 nm). The largest element of the nonlinear tensor is[43] $d_{33} = 21$ pm/V (at 1520 nm) (see Table 1), which is even larger at shorter wavelengths[39] (27 pm/V at 1064 nm). This allows efficient nonlinear parametric three-wave mixing effects such as SHG, sum- and difference-frequency generation (*i.e.,* SFG and DFG) as well as SPDC. Moreover, the broken inversion symmetry of $LiNbO_3$ along with its large nonlinearity bring about a strong electro-optic response, namely the Pockels effect. This effect, wherein an applied external field modifies the refractive index of the material, has already had significant technological impact in integrated photonics and laser technologies, allowing for dynamic light modulators and polarization rotators.

These properties make $LiNbO_3$ an attractive material for photonics applications in general and for nano-optics in particular. However, a significant challenge for uses in nano-optics is posed by the relatively low refractive index, which spans from 2.2 in the near-infrared to 2.4 in the visible spectral range. Yet, the aforementioned properties largely outweigh this drawback in a broad set of applications.

In Table 1, we compare the optical properties of $LiNbO_3$ with other materials commonly used for nonlinear optics and electro-optics at the nanoscale. While semiconducting materials have higher refractive indices and second-order nonlinearities, most of them have limited application in the visible–UV spectral range, due to their typically high absorption. Furthermore, the often-used III–V semiconductors feature a crystalline structure that provides nonlinear coupling only between three different components of the electric field. This feature makes it challenging to take full advantage of their large nonlinearity with co-polarized beams. Finally, $LiNbO_3$ provides unique means for fast dynamic modulation of the material properties by the electro-optic effect, which enables tuning the refractive index by an externally applied voltage with frequencies well-above GHz.[56] It is worth mentioning $BaTiO_3$ as a promising alternative to $LiNbO_3$ for electro-optics applications, thanks to its larger Pockels coefficient. Recently, large electro-optical effects were reported for crystalline $BaTiO_3$ on silicon.[53] $BaTiO_3$ metasurfaces, based on

nanoparticle thin films, and realized by top-down approaches,[57] have been also recently introduced as an alternative to overcome the bottom-up nanofabrication challenges described in the next Section.

3. Nanofabrication of $LiNbO_3$ meta-structures

Due to its strong polar bonds, $LiNbO_3$ is chemically very stable[58] and poses demanding challenges for nanofabrication, especially when the photonic structures need to be fabricated from a thin film. In this Section, we present the recent developments in the nanofabrication of $LiNbO_3$-based platforms (Section 3.1) and discuss novel routes towards further improvement (Section 3.2).

3.1. State of the art in $LiNbO_3$ nanofabrication

We classify nanofabrication methods into two major categories: top-down, whereby parts of the material of interest are deterministically removed; or bottom-up, whereby chemicals assemble into micro- and/or nanostructures. The major milestone for $LiNbO_3$ nanophotonics was the fabrication of thin films with the smart-cut (crystal ion-slicing or ion-cut) technology, which reached the market in the mid-2010s.[59, 60] This brought $LiNbO_3$ back to the attention of various research groups focused on nanophotonics. The smart-cut technique relies on the implantation of He^+/H^+ ions in a well-localized thin layer at a specific depth within the $LiNbO_3$ substrate. In this layer, the crystal structure is modified, which creates an interface where the wafer can be eventually split into two pieces. The depth of the implantation defines the thickness of the future thin film and ranges typically from 400 nm to 1000 nm. The implanted $LiNbO_3$ wafer is then bonded to a SiO_2 film placed on a Si or a $LiNbO_3$ substrate. After thermal annealing, the original $LiNbO_3$ wafer can be split along the "cut" plane. With this method, it is possible to fabricate thin films with different orientation of the crystalline axes, where the extraordinary crystalline *c*-axis can be oriented normal to the thin film (*z*-cut) or parallel to it (*x*-cut or *y*-cut).

For microscale devices based on $LiNbO_3$, such as resonators, waveguides, and modulators, there are several fabrication techniques available,[61] such as proton exchange,[62] ion implantation,[63] femtosecond-laser micromachining,[64, 65], dicing,[66] and metal diffusion.[67] Nonetheless, all these still lack the spatial resolution required to produce $LiNbO_3$ meta-atoms small enough to support resonances at optical frequencies. In

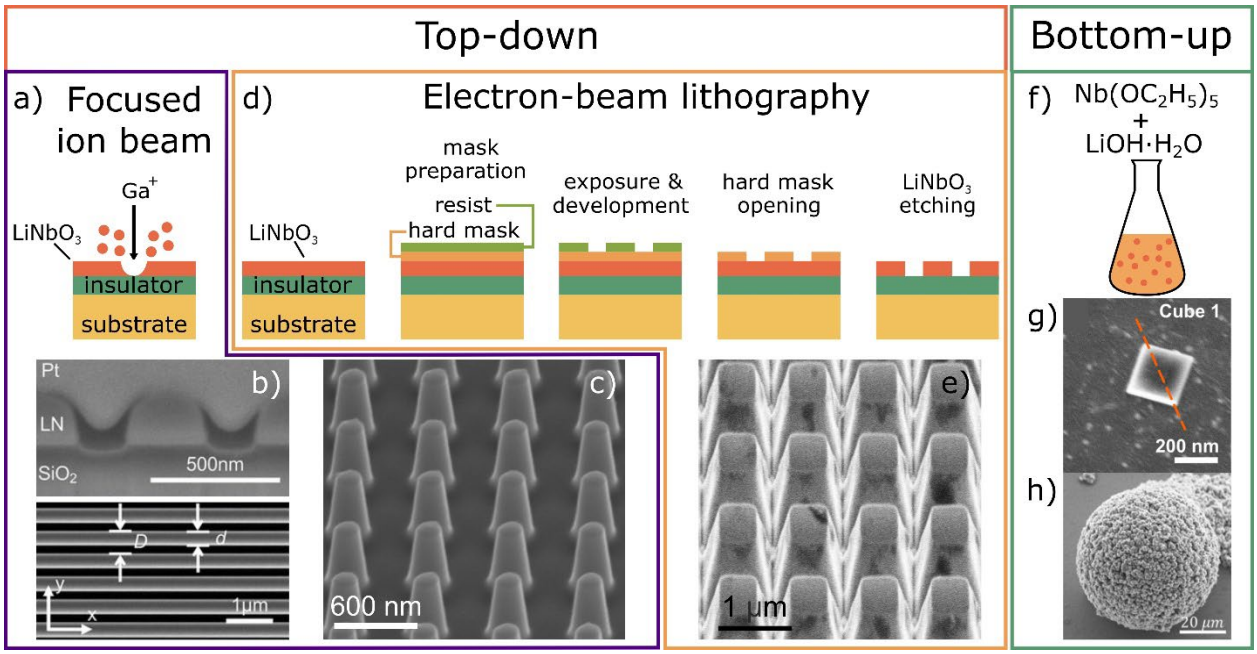

Figure 2. **Overview of fabrication methods and examples of fabricated structures.** (a–e) Top-down methods based on (a–c) focused ion beam (FIB) and (d–e) electron-beam lithography (EBL). (f–h) Bottom-up methods. (a) Sketch of FIB milling. (b,c) Examples of structures obtained by FIB milling: (b) 1D metasurface with nanograting, top—FIB image of the transverse section, bottom—scanning electron micrograph (SEM) image of the nanograting. Reprinted with permission from Ref. 32 © 2019 John Wiley and Sons. (c) SEM of a 2D metasurface. Adapted with permission from Ref. 34 © 2021 The Authors https://creativecommons.org/licenses/by/4.0/. (d) Sketch of the main steps of EBL fabrication. (e) Example of a structure fabricated by EBL: SEM of a 2D metasurface. Adapted with permission from Ref. 33 © 2020 American Chemical Society. (f) Sketch including the essential chemicals for solvothermal synthesis. (g) SEM pictures of a nanocube fabricated by a solvothermal method. Reprinted with permission from Ref. 75 © 2019 American Chemical Society. (h) Crystalline microspheres fabricated by a hydrothermal method (unpublished, courtesy of the authors of Ref. 77).

contrast, focused-ion-beam (FIB) milling and electron-beam lithography (EBL) have already shown convincing results for the fabrication of $LiNbO_3$-based metasurfaces[32–34] and that the quality of the realized nanostructures fulfills the requirements to implement also advanced functionalities.[68–70]

FIB milling uses ions (typically Ga^+) accelerated to energies of around 30 keV to bombard the surface of a material and sputter it, as sketched in Figure 2a. This approach is relatively straightforward, does not require a mask, offers a high resolution (10–15 nm) and produces nanostructures with steep side-walls (≈84°, see Figure 2c).[34,71] However, FIB is based on point-wise ablation, which is time consuming and costly, thus not suitable for nanopatterning large areas approaching the mm^2 scale. Other limitations of FIB are the surface

roughness, which can spoil the resonant performances, and the Ga^+ contamination, which introduces defects within the crystal lattice. These problems can be lessened to some extent by optimizing the FIB operating parameters and by introducing a sacrificial/protective layer that has also the function of preventing charge accumulation and can be removed in a post-processing step.[34]

EBL-based techniques rely on multi-step protocols, akin to those implemented for silicon photonics or electronics (see sketch in Figure 2d). A typical process begins by realizing a hard mask on the wafer to be structured. A tightly focused electron beam is used to directly shape an electron-sensitive organic layer (resist), and in the next step a lift-off process or reactive-ion etching (RIE) can be used to structure a hard mask. Finally, the pattern of the hard mask can be transferred to $LiNbO_3$ via ion-beam etching (IBE), inductively-coupled plasma RIE (ICP-RIE), or RIE.[33, 72] Because, except for the electron beam illumination, all these fabrication steps treat the entire wafer surface at once, EBL can process large sample areas up to several cm^2, which makes it more suitable for wafer-scale processing than FIB. The typical resolution achievable is ~20 nm and the typical side-wall angle for small meta-atoms varies between 70° and 80° (in Figure 2e it is ≈76°). Both parameters as well as the surface roughness limit the achievable quality factors (Q-factor) and strongly depend on the exact fabrication recipe. Therefore, to boost the quality of $LiNbO_3$ metasurfaces, further improvements of the fabrication techniques would be necessary. Indeed, while in silicon metasurfaces the highest reported Q-factor reaches 10^5,[73] $LiNbO_3$ metasurfaces attained only recently values up to 10^3.[74]

Alternatively to the methods based on thin films and deterministic structuring, single $LiNbO_3$ nanoparticles sustaining resonances can also be fabricated through bottom-up approaches.[75–78] This can be achieved with laser ablation,[76] but also several possibilities to produce (crystalline) particles with chemical synthesis were demonstrated: *e.g.* molten salt syntheses,[79, 80] solution-phase synthesis with directed aggregation for controlled growth of crystalline $LiNbO_3$ nanostructures,[81] synthesis of $LiNbO_3$ nanostructures with different morphologies from a single-source precursor by controlling the solvothermal conditions,[82] and increased uniformity synthesis of single-crystalline $LiNbO_3$ nanoparticles by controlled Ostwald ripening.[83] Yet,

these techniques lack the possibility to accurately control the geometry and the size of the grown nanoparticles on length scales above 100 nm, which is crucial for designing nanostructures resonating at specific wavelengths and for obtaining the desired nonlinear and electro-optic parameters, which depend on the size of the nanoparticles,[84, 85] as we will address in Section 4. Additionally, it has been demonstrated that, even for a larger particle size (about 300 nm), bottom-up approaches can affect the crystalline structure leading to a different crystallographic orientation at the surface compared to the bulk.[86, 87] This might favor spurious surface effects and reduce the effective nonlinearity. Precise positioning of nanoparticles is another issue, and only recently viable routes were demonstrated, *e.g.* by parallel capillary stamping[88] and by imprinting or FIB-structuring of spin-coated nanoparticle films, where the randomly oriented nanoparticles are embedded inside a high-index filling material forming a nonlinear composite.[57] Hence, even when starting initially from bottom-up synthesis, for applications relying on the deterministic location of nanoresonators, FIB- and EBL-based approaches currently represent the most promising and reliable techniques.

3.2. Enhancing $LiNbO_3$ functionalities

Thin-film $LiNbO_3$ is routinely used as a material for integrated optics, where several strategies to further enhance its capabilities were already introduced,[28, 89–91] some of which can also profitably be translated to nanophotonics.

3.2.1. Doping

For crystals such as $LiNbO_3$, doping can be used to tailor their properties.[92] For example, doping with MnO alters the energy levels of $LiNbO_3$, pushing its absorption further to the UV or to the MIR[93] or modifying its refractive index.[94] However, the characteristic refractive-index variations achieved are of the order of 10^{-3} and will not sizably improve light confinement (and hence the Q-factor) in $LiNbO_3$ nanophotonic applications, which is typically fostered by large refractive-index differences between the nanostructures and their surroundings.

Transition-metal ions like Fe, Cu, and Mn are used as dopants to increase the photorefractive effect, i.e. the change of the refractive index due to irradiation with light.[95–97] This could be used to realize dynamically tunable nanophotonic elements. On the other hand, doping $LiNbO_3$ with metal ions like Mg, Zn, In, Sc, Hf, Zr, Sn strongly reduces photorefraction, enabling radiation-stable optical elements by reducing the laser-induced optical damage.[98] Fabricating metasurfaces from films with these dopants will raise their photodamage threshold, especially when used with CW lasers.

Rare-earth dopants like Er, Yb, Tm can act as fluorescent emitters when embedded in $LiNbO_3$, extending the material functionality.[90, 91] Many works exploited Er and Yb for lasing in $LiNbO_3$ microdisks[99,100] and waveguides[101–103]. In perspective, $LiNbO_3$-metasurface lasers have the potential to decrease the lasing threshold and improve the directionality of the emission. Furthermore, the mentioned ions can act as single-photon emitters and therefore enable quantum light sources based on $LiNbO_3$.

3.2.2. Periodic poling

$LiNbO_3$ is a ferroelectric crystal, namely, it can possess a spontaneous nonzero polarization even in the absence of an external electric field. This is a consequence of the lack of inversion symmetry of the lattice, which leads to the separation of positive and negative charges. When a strong electric field is applied along the crystalline *c*-axis, it is possible to displace the Li and Nb ions and thus to permanently invert the spontaneous polarization in a process called electric-field poling.[104] This also leads to a sign change in the nonlinear susceptibility $\chi^{(2)}$. Based on this effect, second-order nonlinear effects in $LiNbO_3$ can be controlled, *e.g.*, by applying this procedure to some parts of a $LiNbO_3$ thin film to create periodic or aperiodic poling patterns, which results in a spatially-structured $\chi^{(2)}$ nonlinearity. For metasurfaces this is especially interesting for *x*-cut or *y*-cut films (as the *c*-axis lies into the plane of the film) to facilitate nonlinear processes seeded by a propagating beam impinging at normal incidence with respect to the device.

Periodic poling of $LiNbO_3$ thin films was already employed to support quasi-phase-matching of SHG in waveguides.[105–107] Moreover, recent advances in the poling algorithms demonstrated sub-μm poling

periods[108] matching the scales of the poling to the relevant scales in metasurfaces. Such nonlinearity engineering can be achieved at a subwavelength scale using electron-beam direct writing[109] or high-voltage scanning-probe microscopy.[110] State-of-the-art works achieve poling periods as small as 600 nm for *x*-cut[108,111,112] and 300 nm for *z*-cut[113] $LiNbO_3$ thin films. Therefore, using electric-field poling one can engineer the nonlinearity at a subwavelength scale. As this is not easily achievable for other materials, $LiNbO_3$ offers a unique opportunity to create a new class of optical metasurfaces with simultaneous spatial variations of the linear and the nonlinear properties. Adding this degree of freedom for manipulating the nonlinearly generated field in frequency-conversion processes could enable novel applications of metasurfaces for nonlinear beam generation and steering. First steps in this direction were demonstrated recently in a $LiNbO_3$ metasurface for SHG, which due to the poling-induced nonlinear grating showed additional diffraction orders.[114]

4. $LiNbO_3$ metasurfaces for nonlinear, quantum, and electro-optics.

The progress in nanofabrication technologies described in Section 3 enables the realization of $LiNbO_3$-based metasurfaces with nanometric spatial features, facilitating the deployment of innovative platforms for nonlinear and electro-optic applications in the visible to NIR spectral range. In particular, the main applications that we foresee for $LiNbO_3$ in meta-optics are the realization of subwavelength-thick devices for efficient or broadband light conversion (see Section 4.1) and ultra-compact entangled-photon sources for quantum optics (see Section 4.2). In addition, the strong electro-optic coefficient of the material, which has already made $LiNbO_3$ a key player in integrated electro-optics, can be further exploited to enable nonlinear light modulation in metasurfaces by external driving fields (see Section 4.3).

4.1. Nonlinear optics with $LiNbO_3$ metasurfaces

4.1.1. Second-harmonic generation enhancement

Nonlinear wave mixing in nanostructured materials can be described as coupling between resonant modes of the structure, excited at different wavelengths. These are often described as the quasi-normal modes of the structure.[115] In contrast to larger-scale microstructures, in nanostructured materials such as

metasurfaces, the modes often involve all three electric field components—see Eq. (4.1)—with similar amplitudes. The nonlinear polarizations generated by mixing these field components via the *n*-th order susceptibility tensor $\chi^{(n)}$ of the material are the primary sources of the nonlinear optical signal. Here we mainly focus on second-order nonlinear interactions ($n = 2$).

In quadratic nonlinear materials such as $LiNbO_3$, SHG is usually the most prominent nonlinear process, corresponding to the mixing between two impinging fields of angular frequency ω mediated by $\chi^{(2)}$. In general, the efficiency of SHG is governed by the cross-coupling coefficient κ. Within nanoresonators, one has a complex field distribution, and κ is a function of the spatial overlap integral between the electric field of the optical resonant mode (E^{ω}) at the impinging frequency ω and that ($E^{2\omega}$) at the generated frequency 2ω computed over the volume V of the nanostructure

$$\kappa \propto \left| \sum_{ijk} \chi^{(2)}_{ijk} \int_V E_i^{2\omega^*}(\mathbf{r})\, E_j^{\omega}(\mathbf{r})\, E_k^{\omega}(\mathbf{r})\, \mathrm{d}\mathbf{r} \right|^2 \qquad (4.1)$$

where the indices *i*,*j*,*k* run over the Cartesian components *x*,*y*,*z*. In bulk and guided optics, κ can be largely simplified, leading to the well-known phase-matching condition. Conversely, in nano-optics, κ depends on the mode fraction that is contained within *V*. Such requirement on the mode fraction along with the presence of all the electric field components makes the optimization of κ a major design task in nonlinear meta-optics [116 117]. As the fields inside the nanostructures are enhanced proportionally to the quality factor of the resonances, the SHG efficiency defined as the input/output power ratio $\eta^{\mathrm{SH}} \equiv P^{2\omega}/P^{\omega}$ can be also expressed as $\eta^{\mathrm{SH}} \propto \kappa Q_{\mathrm{FW}}^2 Q_{\mathrm{SH}}$, where Q_{FW} and Q_{SH} are the quality factors at the fundamental wave (FW) and the second harmonic (SH) wave, respectively. We note that the conversion efficiency depends quadratically on the Q-factor of the FW resonance, hence sharp resonances at the pump frequency are most critical for efficient second-harmonic generation. On the other hand, one must ensure that the spectral bandwidth of the resonances equals or is larger than that of the excitation pulses, so to couple effectively the incident energy into the resonant mode. Finally, since SHG is strongly influenced by the symmetry of the material and the nanostructure along with the quasi-normal modes in the nanostructure, the SHG

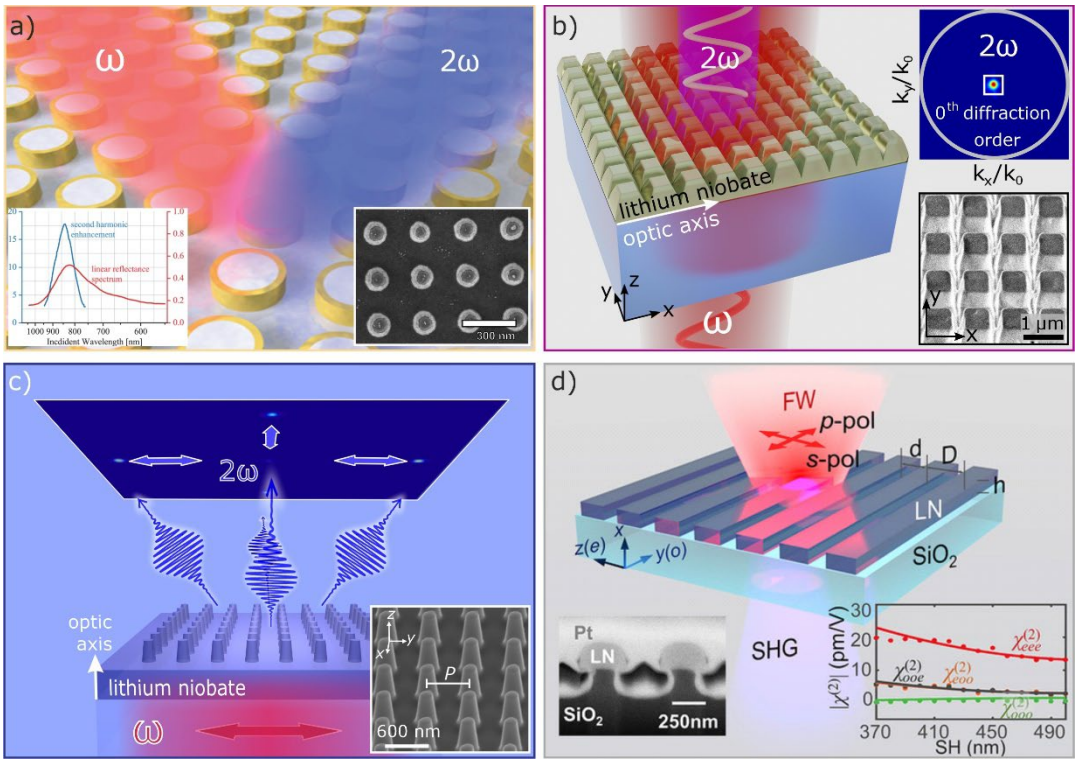

Figure 3. **Nonlinear metasurfaces based on $LiNbO_3$ for SHG enhancement and steering.** (a) Plasmonic nanoring metasurface integrated on *x*-cut $LiNbO_3$ substrate. ω and 2ω denote the angular frequency of the pump and SHG emission, respectively. Adapted with permission from Ref. 121 © 2015 American Chemical Society. (b,c) Mie-resonant $LiNbO_3$ metasurface obtained by nano structuring (b) a thin *x*-cut $LiNbO_3$ film (adapted with permission from Ref. 33 © 2020 American Chemical Society) and (c) a thick *z*-cut $LiNbO_3$ substrate (adapted with permission from Ref. 34 © 2021 The Authors https://creativecommons.org/licenses/by/4.0/.) The bottom-right insets in (a,b,c) display scanning electron micrographs of the metasurfaces. The top-right inset in (b) and the dark blue frame in c) show back focal plane images of the SHG emission in the Fourier space. (d) $LiNbO_3$-based 1D photonic grating. Reprinted with permission from Ref. 35 © 2021 John Wiley and Sons.

emission is often characterized by non-trivial polarization and directional properties. This was widely explored for individual $LiNbO_3$ nanostructures, including nanowires,[118] waveguides,[119] nanocubes,[75] nanospheres,[76] and nanodisks.[120] In metasurfaces there are additional constraints imposed by the symmetry of the underlying arrangement of the meta-atoms, which may alter the mode structure in the near field and filter directionally the emission of the isolated meta-atom, thereby shaping the SHG emission in the *k*-space and leading to the appearance of diffraction orders.[25, 26]

Sample [(1)]	λ_{FW} (nm) [(2)]	λ_{SH} (nm) [(3)]	Q_{FW} [(4)]	I_{FW}^{pk} (GW/cm^2) [(5)]	$\eta \equiv P_{SH}/P_{FW}$	$\gamma \equiv P_{SH}^{pk}/P_{FW}^{pk\ 2}$ (W^{-1})	$\xi \equiv \eta/I_{FW}^{pk}$ (cm^2/GW)
Experiments							
2D MS [33]	1550	775	~100	4.5	9.00E-07	2.43E-10	2.00E-07
2D MS [34]	830	415	~10	0.5	2.53E-08	2.86E-11	5.05E-08
1D MS [35]	820	410	~50	2.05	1.98E-06	1.39E-09	9.64E-07
1D DBR MS [74]	1548	774	~2000	0.002	4.09E-08	3.02E-09	2.13E-05
Simulations							
2D MS [30]	820	410	~20	1	5.00E-05	-	5.00E-05
1D BIC MS [31]	690	345	~10000	1.33	8.13E-05	-	6.11E-05
2D stack BIC MS [122]	1334	667	~1000	5.3	1.30E-04	-	2.45E-05
2D BIC MS [123]	801	400.5	~80000	3.3E-06	4.90E-03	-	1.48E+03
2D MS on Au [124]	800	400	~40	3.4	5.00E-04	-	1.47E-04

Table 2. SHG performances of $LiNbO_3$ metasurfaces. Notes: (1) 1D: one-dimensional; 2D: two-dimensional; MS: metasurface; DBR: distributed Bragg reflector; BIC: bound state in the continuum. (2) λ_{FW}: wavelength of the fundamental (pump) wave (FW). (3) λ_{SH}: wavelength of the second-harmonic (SH) emission. (4) Q_{FW}: quality factor at the FW. (5) I_{FW}^{pk}: pulse peak intensity of the FW field calculated as average input power (P_{FW}) divided by the spot size on the metasurface.

The first exploration of $LiNbO_3$ metasurfaces for enhancing SHG involved plasmonic resonant modes supported by gold rings surrounding small $LiNbO_3$ nanopillars,[121] as shown in Figure 3a. The nanopillars were etched in a monolithic substrate of *x*-cut crystalline $LiNbO_3$. The use of the *x*-cut material allowed to easily exploit the strongest nonlinear tensor component, namely d_{33}. A nearly 20-fold SHG increase was observed with respect to the unstructured substrate, showing the potential of strong SHG enhancement by nanostructuring the $LiNbO_3$ material.

The development of thin-film $LiNbO_3$ by ion slicing has sparked new opportunities for its employment in nanophotonics and meta-optics. This was first applied in conjunction with waveguides, where gradient silicon metasurfaces allowed achieving phase matching-free SHG.[10] However, the big opportunity lied in exciting resonant modes within the $LiNbO_3$ itself without resorting to further hybrid integration. In Ref. 33, by nanostructuring an *x*-cut $LiNbO_3$ thin film with the appropriate geometry, electric- and magnetic-type dipolar resonances were excited in a metasurface at a telecommunication wavelength, see Figure 3b. The largest SHG efficiency (row 1 in Table 2) was observed for the resonance dominated by the electric dipole contributions because its field distribution best exploited the largest nonlinear tensor element, d_{33}.

Due to the strongly hybridized modes, a fundamental advantage of resonant metasurfaces is their ability to generate strong longitudinal fields, which is not possible in bulk crystals. In metasurfaces one can thus access nonlinear tensor components that otherwise cannot be directly excited. For example, *z*-cut $LiNbO_3$ can be used to fabricate resonant metasurfaces with highly enhanced harmonic generation.[34] Figure 3c shows such a metasurface fabricated on a monolithic $LiNbO_3$ substrate and operating in the visible spectral range.[34] The SHG process in this metasurface was enhanced by a magnetic-type Mie-resonance and resulted in the emission of blue light at ~415 nm with negligible self-absorption.

While the *x*-cut metasurface designs showed strong zeroth order emission (see top-right inset in Figure 3b), the *z*-cut metasurface emits predominantly in the first diffraction orders (Figure 3c), whose relative power can be modulated via the pump polarization, as the emission is dominated by two diffraction orders oriented along it. These metasurfaces exhibited a SHG conversion coefficient $\gamma = P_{\mathrm{SH}}^{\mathrm{pk}} / \left(P_{\mathrm{FH}}^{\mathrm{pk}}\right)^2$ up to 10^{-10} W^{-1}, where P^{pk} is the pulse peak power (row 1 and 2 in Table 2). A similar SHG efficiency at visible wavelengths has also been found in 1D Mie-resonant nano-gratings based on an *x*-cut $LiNbO_3$ thin film, see Figure 3d[35] and row 3 of Table 2. The 1D structures show a large polarization anisotropy. SHG enhancement at different visible wavelengths can be achieved by changing the width of the $LiNbO_3$ grating stripes.

However, the requirement that the Mie-resonant optical modes couple to free-space propagating light (which corresponds to radiative losses), along with the moderate refractive index of $LiNbO_3$, results in low Q-factors (Q~10) of the resonances. Such low values stand in stark contrast to thin-film $LiNbO_3$ integrated optical components, such as microdisk resonators[125] and photonic crystal resonators.[126] Therefore, the SHG enhancement in Mie-resonant $LiNbO_3$ metasurfaces was so-far quite limited.

To further enhance the SHG conversion efficiency, it is possible to utilize high Q-factor modes based on the concept of bound state in the continuum (BIC).[127, 128] This possibility has been theoretically explored, suggesting that a strong SHG enhancement can be achieved by controlling the coupling to free-space radiation through symmetry breaking and excitation of quasi-BIC modes[31, 122, 123] (see rows 6–8 in Table 2). In particular, the concept of etchless $LiNbO_3$ metasurfaces—namely, periodic structures realized onto otherwise unstructured films of $LiNbO_3$—has been introduced[42, 129, 130] to avoid the complex etching process of $LiNbO_3$ while granting access to highly delocalized resonances with high Q-factors. This concept has been recently tested experimentally in x-cut etchless $LiNbO_3$ metasurfaces, demonstrating experimental quality factors of Q = 455 and an over 50 times enhancement of SHG in comparison to the bare $LiNbO_3$ film.[42] We note that as the BIC modes consist of transversely propagating waves, they are strongly affected by the finite transverse size and edges of the metasurfaces. Interestingly, recent experiments have shown that the implementation of a heterostructure cavity can mitigate the transverse leakage of energy and further boost the Q-factors of the metasurfaces (to over 5,000), thereby dramatically enhancing the SHG processes, though at the expense of a reduced bandwidth[74] (see row 4 in Table 2). However, compared to fully etched $LiNbO_3$ metasurfaces, etchless structures provide only limited control of the local mode-fields overlapping with the nonlinear material.

Table 2 summarizes the SHG performances of some key experimental and numerical works on $LiNbO_3$ metasurfaces. The performance is quantified by different parameters: the nonlinear conversion efficiency η, the conversion coefficient γ, and the nonlinear coefficient ξ, all defined in the table header. η is the most commonly employed parameter representing how much of the input power is nonlinearly converted to the

output; hence η depends on the input laser power, repetition rate, and focusing. In contrast, γ is an absolute parameter that solely reflects the nonlinear properties of the sample and, as such, it better represents the effective nonlinear susceptibility of the characterized system.

4.1.2. Perspective applications to nonlinear meta-optics

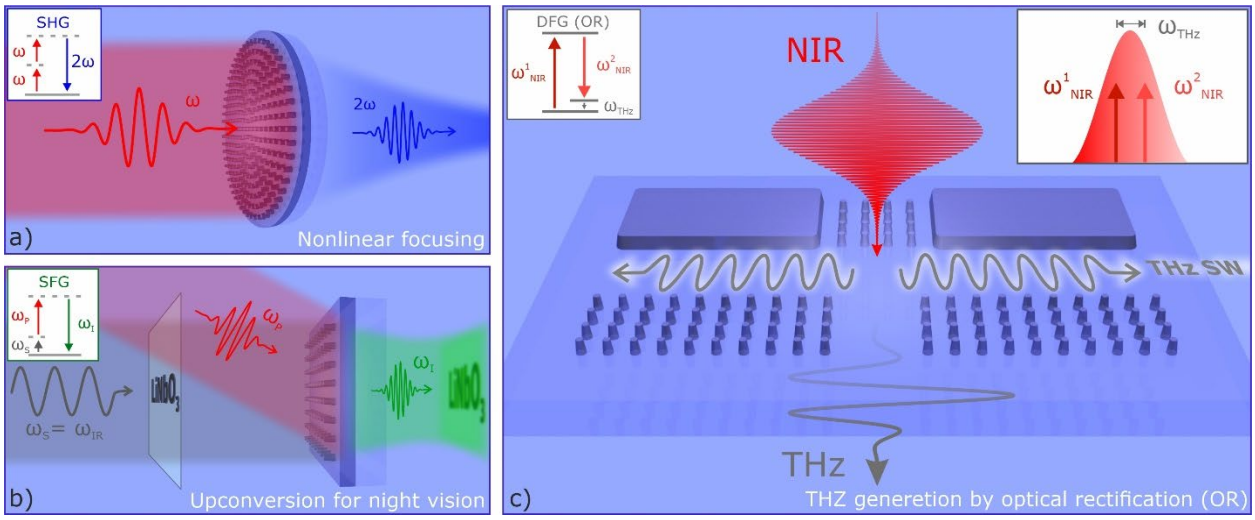

Figure 4. Perspectives and applications of nonlinear metasurfaces based on $LiNbO_3$. (a) Sketch of a $LiNbO_3$ monolithic metalens focusing SHG light onto a sample, for noninvasive coherent imaging. (b) Sketch of a $LiNbO_3$ metasurface designed to upconvert infrared radiation to the visible by SFG with a second visible light beam for night-vision application (similar to Ref. 136). (c) Concept of a nonlinear $LiNbO_3$ metasurface for generating THz radiation by optical rectification (*i.e.*, DFG), exploiting a doubly resonant mechanism based on the Mie/lattice resonances of the meta-atom array and the design of a THz dipole meta-antenna. This concept can also exploit the strong phonon-polariton resonances supported by $LiNbO_3$ in the region between 5 and 15 THz.

We expect that these first important milestones in SHG enhancement by means of $LiNbO_3$-based platforms will boost the development of nonlinear meta-optics, spanning the whole visible up to the MIR range. We believe that these latest conceptual and experimental achievements will further nourish the efforts of researchers in the field of nanofabrication, hence creating a positive feedback effect towards improved platforms. In particular, $LiNbO_3$-based platforms for enhanced SHG will find a fertile ground in the ever-expanding field of molecular sensing, where $LiNbO_3$ chips and waveguides have been already applied successfully for optical[131–133] and electro-optical[134] sensing. In fact, the enhanced integration enabled by $LiNbO_3$ meta-optics along with the exploitation of ultra-narrow optical resonances (*e.g.*, quasi-BIC modes)

and the nonlinear character of SHG, if employed as a probe, can potentially enhance the sensitivity and scalability of these platforms.

In addition, phase engineering of the nonlinear emission by the metasurface can enable nonlinear wavefront shaping, hence steering, and even focusing *e.g.*, the SHG (see Figure 4a). In this regard, poling provides an additional mechanism for shaping the nonlinearly generated light[114] and gives $LiNbO_3$ an edge in comparison to most other metasurface platforms. Spatial shaping is indeed a key feature towards the realization of nonlinear phase plates and metalenses.[135] Nonlinear metalenses may open new routes to nonlinear microscopy; for example, they can be applied to upconvert infrared propagating beams into visible–UV light and focus it for *in-situ* microscopy.

Among the many applications envisioned for frequency conversion in nonlinear metasurfaces, one of the most fascinating is enhanced night vision. Although still based on proof-of-principle applications involving mainly ultrashort pulses, the possibility to upconvert light from the infrared to the visible range, where cheap cameras and even the naked eye can be employed for detection, is extremely appealing. Some recent works demonstrated the possibility of translating infrared radiation to the central region of the visible spectrum by SFG[136, 137] and THG[138] by means of dielectric metasurfaces and nanostructures. Given its broad transparent spectral window, $LiNbO_3$-based nonlinear meta-optics offers exciting perspectives for such an application (see Figure 4b).

Additionally, $LiNbO_3$ features lattice vibrational modes (optical phonons) in the THz range that can strongly couple to electromagnetic fields giving rise to phonon polaritons.[139, 140] $LiNbO_3$ has been already successfully employed for THz management as a bulk crystal[141] or in thin films[142] in the THz region (< 1 THz). Recently, Benea-Chelmus and co-workers demonstrated an on-chip hybrid system based on thin-film $LiNbO_3$ coupled with THz antennas to generate and shape at-will the temporal, spectral, phase, and far-field characteristics of the THz radiation, by designing low-loss on-chip components.[143] Although the operation in the THz gap region (1–10 THz) is limited by the strong material absorption, the employment of $LiNbO_3$-based metasurfaces may ensure efficient generation and shaping of THz radiation in this region

by optical rectification, thanks to the enhanced linear and nonlinear response provided by the phonon polaritons. THz sources in this frequency range can be strategical to investigate materials' crystal structure and its dynamics[144] and to perform vibrational spectroscopy of macromolecules.[144–146] We also expect a distinct impact of these technologies, given the promising applications of THz radiation in biology and medicine[147, 148] and for the detection of explosives, weapons and drugs in security applications.[149] In this framework, a seminal work recently demonstrated the capability of $LiNbO_3$-based metasurfaces to efficiently generate broadband THz radiation around 1 THz.[150] Yet, the THz gap region remains widely unexplored. The technological advances in nanofabrication together with its high nonlinear coefficient and unique phononic features single out $LiNbO_3$ metasurfaces as a privileged starting point for the development of THz sources seeded by optical rectification (see Figure 4c).

Finally, by exploiting the strong quadratic nonlinearity of the material, cavity-free all-optical switching was recently demonstrated in $LiNbO_3$ nanowaveguides[151] at ultra-low switching energies and ultrafast operation times. This was achieved by engineering dispersion and quasi-phase matching by material poling in the nanowaveguides. We envisage the enticing possibility to translate this concept to $LiNbO_3$ meta-optics, thanks to the latest development in nanoscale poling (see Section 3).

4.2. Quantum optics with $LiNbO_3$ metasurfaces

4.2.1. Engineering spontaneous parametric down-conversion

Many quantum applications like quantum cryptography, quantum computing, and quantum information make use of photon pairs, namely quantum states of light containing two correlated photons. The generation of such pairs relies mainly on the second-order nonlinear process of SPDC.[152] In SPDC, one pump photon spontaneously decays into two daughter photons, named signal and idler, with their wavelength being determined according to energy conservation and the field overlap with the source. However, while phase matching permits the interaction of the propagating modes with large volumes of the nonlinear material, achieving significant generation rates in ultra-thin metasurface is a fundamental challenge due to the intrinsically low amount of material involved.

For SPDC, nanostructures offer broader angular and spectral emission ranges of the generated photon pairs,[153,154] as well as a smaller footprint[28] as compared to bulk components. First experiments with a 300 nm *x*-cut $LiNbO_3$ thin film showed a photon-pair rate of 0.3 Hz/mW with a spectral bandwidth above 500 nm (see Figure 5a,b).[155] In contrast to thin films, metasurfaces exploit resonant field enhancement to boost photon-pair generation and enable wavefront manipulation to improve collection efficiency and enable routing.[156] Several works have already suggested using metasurfaces for generation, manipulation and detection of quantum states,[19, 157, 158] some of them concentrating on III–V semiconductors (GaAs, AlGaAs)[159–161] and silicon.[162] These results show that metasurfaces offer benefits also for quantum optics.

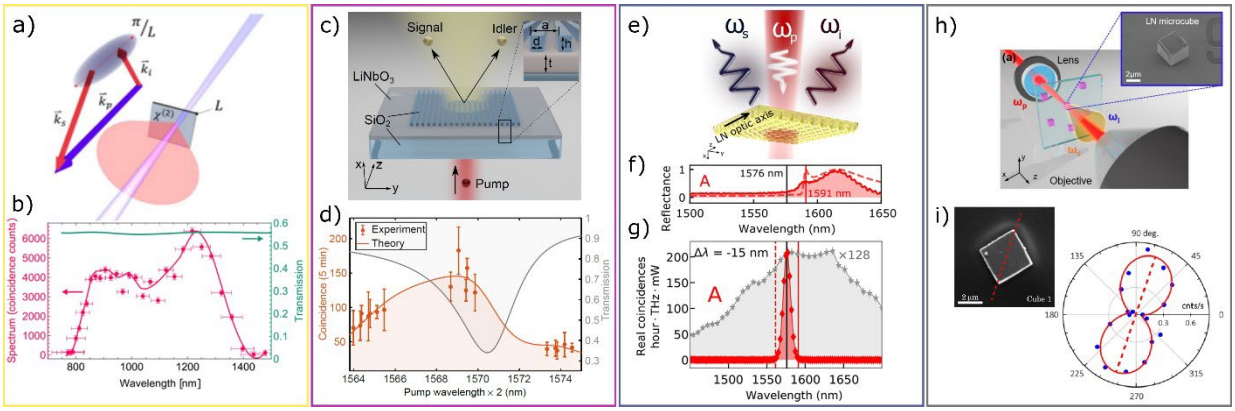

Figure 5. SPDC in $LiNbO_3$—state of the art. (a) Scheme of relaxed phase-matching condition and broadband SPDC generation from subwavelength nonlinear films. Reprinted in part with permission from Ref. 153 © 2019 American Physical Society. (b) Measured SPDC spectrum of photon pairs generated in a 300 nm-thick *x*-cut $LiNbO_3$ film pumped at 515 nm (pink dots) with pink line as a fit for detection efficiency. The green line is the calculated transmission of the Fabry–Pérot etalon formed by the $LiNbO_3$ film. Reprinted with permission from Ref. 155 © 2019 The Optical Society. (c) Scheme of SPDC by an etchless metasurface on thin-film $LiNbO_3$. (d) Coincidence histograms of SPDC for different pump wavelengths (orange dots) and numerically calculated SPDC (orange line). Grey line—transmittance spectrum of the metasurface exhibiting a resonance. Panels c,d are reprinted with permission from Ref. 42 © 2022 The Authors https://creativecommons.org/licenses/by-nc/4.0/. (e) Scheme of SPDC generation in reflection by a $LiNbO_3$ metasurface. (f) Measured and calculated reflectance spectra of the $LiNbO_3$ metasurface. (g) Measured SPDC spectrum pumping at 1591 nm the metasurface (red) and thin-film $LiNbO_3$ (grey). Panels e–g are adapted with permission from Ref. 41 © 2021 The Authors https://creativecommons.org/licenses/by/4.0/. (h) Scheme of SPDC in transmission from a single $LiNbO_3$ nanocube and (i) measured coincidence histogram for pump polarization parallel (red) and perpendicular (black) to the $LiNbO_3$ optic axis (red). Panels h,i are reprinted with permission from Ref. 164 © 2022 Optica Publishing Group.

An etchless $LiNbO_3$ metasurface incorporating a SiO_2 grating (see Figure 5c) was applied to generate frequency-degenerate entangled photon pairs at telecom wavelengths via SPDC.[42] Here, resonant enhancement of the photonic density of states led to higher generation rates when degenerate signal and idler wavelengths were close to the grating resonance, as shown in Figure 5d. Furthermore, silver nanogratings on thin-film $LiNbO_3$ sustaining plasmon-polariton resonances at different wavelengths were numerically shown to mediate non-degenerate SPDC,[163] but the metal-induced losses decreased the achievable conversion efficiency (see row 6 in Table 3). Metasurfaces from nanostructured thin-film $LiNbO_3$ were also used for photon-pair generation (see Figure 5e).[41] This work[41] revealed that the width of the SPDC spectra can be controlled by tuning the pump wavelength away from the resonance (see Figure 5f,g)): thus, resonant metasurfaces have the potential to control the SPDC spectra (see row 3 in Table 3).

Even single nanoparticles like $LiNbO_3$ colloidal cubes have been shown to generate photon pairs (see Figure 5h,i).[164] Here, the overlap between resonances at the pump and SPDC wavelengths led to an enhanced generation efficiency (see row 5 in Table 3).

Platform	Thickness (μm)	Power (mW)	SPDC rate (1) Hz/(mW·μm)	SPDC rate (2) mHz/(mW·μm^3)	SPDC spectral width
$LiNbO_3$ film [153]	~6	220	1.06	13.5	500 nm
$LiNbO_3$ film [155]	0.3	9	1.04	–	500 nm @515 nm pump
$LiNbO_3$ metasurfaces [41]	0.68	70	0.11	6.1	10÷40 nm (3)
$LiNbO_3$ slab + SiO_2 grating [42]	0.304	85	0.07	0.009	3 nm (theory)
$LiNbO_3$ nanocube [164]	3.6	50	0.007	0.57	–
$LiNbO_3$ slab + silver grating (simulations) [163]	0.306	5 (4)	915 (5)	1.17 (5)	1 nm (5)

Table 3. Summary of measured and numerically calculated SPDC properties. Notes: (1) Rate normalized to pump power and $LiNbO_3$ thickness. (2) Rate normalized to pump power and $LiNbO_3$ volume. (1,2) are detected rates, losses in collection/detection are not accounted for. (3) The spectral width depends on the detuning of the pump from the resonance. (4) Calculated from intensity 1 W/cm^2 for the metasurface with size 1 mm^2. (5) SPDC rate is normalized to the bandwidth of 1 nm.

Table 3 summarizes the recent literature on SPDC from $LiNbO_3$ nanostructures and metasurfaces. Owing to its high transparency, $LiNbO_3$ has a significant advantage over semiconductor materials in terms of coincidence-to-accidentals ratio (CAR) of the observed two-photon statistics. Indeed, the CAR reported in $LiNbO_3$ thin films and metasurfaces exceeds by an order of magnitude that observed in compounds such as GaP and GaAs. However, despite the obvious experimental breakthrough of demonstrating SPDC, the current rate of generated photon pairs in $LiNbO_3$ metasurfaces and nanostructures is still low. In future experiments, advanced designs based on BIC resonances[165] or coupled Mie/BIC modes with Bragg resonances can boost the electromagnetic fields inside the resonators by improving the coupling with the resonators and/or increasing the effective interaction length.[166] Additionally, further developments of the etchless approach demonstrated by Zhang et al.[42] may increase the SPDC generation efficiency thanks to the use of larger volumes of the nonlinear material. Controlling the SPDC emission direction is yet another way to increase the number of detected photon pairs, where optimized design can help to improve the directionality so that more photons can reach the detector; to-date, particular efforts towards this direction are still required. After the first success of photon-pair generation, a lot of efforts have been dedicated to demonstrating entanglement. Recently, polarization entanglement in a subwavelength film,[167] momentum entanglement in a metasurface,[42] and approaches for cluster-state generation through spectral entanglement were reported.[165]

4.2.2 Perspective applications to quantum meta-optics

In perspective, metasurface-based sources are a promising platform to create hyperentangled states, where different degrees of freedom, such as orbital angular momentum, propagation direction, wavelength, and polarization, are simultaneously entangled thanks to the high flexibility of control granted by meta-optics. Furthermore, as every single meta-atom in a metasurface can be considered as an independently addressable source of photon pairs, very high-dimensional photon-pair states become possible. The potential of this approach has been demonstrated already by combining a metasurface, which controls the pump beam, with a bulk nonlinear crystal.[159] Such high-dimensional states are an important resource for applications for

quantum information processing. However, to unlock these possibilities, several conceptual and experimental challenges remain to be solved.

In particular, a dedicated design of multi-parameter metasurfaces for quantum-state control demands appropriate methods to calculate quantum processes in nanostructures both analytically and numerically. The approaches typically used for integrated or bulk optics can only be partially applied to metasurfaces, which are open resonators with absorption. To-date, among the various tools that are being developed, quantum–classical correspondence between SPDC and SFG was used to assess the first experimental results[41, 42, 164, 168] and suggest new designs [160, 163]. A more rigorous approach is based on the Green's function method[169] for constructing two-photon amplitudes, which was shown to be able to calculate efficiency and directionality of photon-pair generation from a single spherical nanoresonator.[170] But this method is hardly applicable to metasurfaces as it requires a rigorous description of the modal decomposition in terms of multipoles. A more general approach also based on Green's functions uses the quasi-normal modes formalism to describe nonlinear nanoresonators[115] and has great potential to describe SPDC in metasurfaces.[171]

Besides photon pairs, also single photons are often used as non-classical states of light and can profit from the ability of metasurfaces for complex manipulations. Single photons are typically generated by atom-like emitters.[172–174] Although pure $LiNbO_3$ does not host the color centers typically employed for this task in

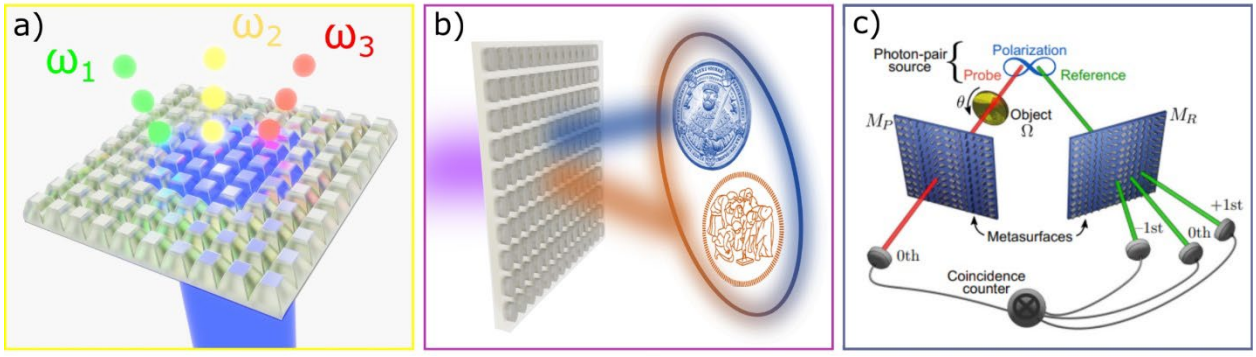

Figure 6. Perspectives and applications of metasurfaces based on $LiNbO_3$ for quantum optics (a) Concept of a metasurface for single-photon generation. (b) Concept of a metasurface creating entangled images with photon pairs. (c) Concept of a metasurface for polarization ghost imaging.[177, 178] Panel c is reprinted with permissions from Ref. 177 © 2021 American Physical Society.

solid-state systems, selective doping with rare-earth ions (Er, Tm, Yb) could provide such emitters. Moreover, $LiNbO_3$ can be integrated with III–V semiconductor quantum dots[89] or transition metal dichalcogenides[175] emitting single photons. In fact, $LiNbO_3$ is a very suitable material that, due to its large transparency range, is compatible with many different emitters. Furthermore, one can take advantage of heralding to obtain single photons from photon pairs generated by SPDC, where one photon from a pair is used for quantum applications, while the second photon "heralds" its presence.

We anticipate that in the coming years quantum optics at the nanoscale will rapidly develop and give birth to many new devices and applications. Of course, also several other materials are being considered,[176] but $LiNbO_3$ is one of the most promising platforms due to its combination of properties. Figure 6 illustrates some of the most enticing perspective applications of $LiNbO_3$ metasurfaces, e.g. a demonstrates single-photon generation and manipulation via single metasurface, b depicts the generation of entangled images, where another degree of freedom was added—the spatial domain, to obtain a complex spatially entangled state, and c shows the concept of metasurface-aided polarization ghost imaging of an object, where one detector senses photons interacted with the object and transmitted through the metasurface, and a set of detectors senses the photons that have never "seen" the object but were diffracted by the another metasurface.[177] In particular, the control over the parameters of the transmitted light can be coupled with the ability to generate photon pairs by SPDC, which in quantum optics enables advanced projective measurements with the potential to realize schemes for tailoring photonic quantum states.[162, 177, 178]

4.3. Electro-optics with $LiNbO_3$ metasurfaces

4.3.1. Electro-optical modulation with ultra-thin optical devices

The electro-optic (EO) effect, *i.e.* Pockels effect, is the most widely exploited feature of $LiNbO_3$, especially in integrated photonic circuits. This second-order nonlinear process consists in the variation of the refractive index induced by a static (or low-frequency) electric field. The refractive-index modulation depends linearly on the amplitude of the applied static field. The effect is maximized when the static electric field is oriented parallel to extraordinary crystalline *c*-axis. For small index changes one can approximate

$$\begin{cases} \Delta n_{\mathrm{e}} = -\frac{1}{2} n_{\mathrm{e}}^3 \, r_{33} E_z \\ \Delta n_{\mathrm{o}} = -\frac{1}{2} n_{\mathrm{o}}^3 \, r_{13} E_z \end{cases} \tag{4.2}$$

where E_z is the amplitude of the externally applied static electric field, while r_{33} = 31 pm/V and r_{13} =8 pm/V are the relevant EO coefficients at a wavelength of 500 nm.[44, 45] Harnessing this phenomenon has enabled the development of waveguide-based integrated EO modulators that are crucial for high-speed telecommunication networks.[179,180] EO modulation is also attractive for devising new dynamic metastructures compatible with free-space optical components, operating at GHz modulation rates.[181] This opportunity is currently attracting large interest.[36–38] Indeed, a modulation of the refractive index can spectrally shift a resonant mode and, consequently, modify the optical response of a metasurface. However, the resulting modulation of the refractive index is limited by the dielectric strength, which in $LiNbO_3$ corresponds to 65 kV/mm but reduces to 3 kV/mm in air.[182] Thus, the achievable refractive index modulation in the visible to NIR spectrum is of order 10^{-4}. In the context of EO waveguide-based modulators, this limitation is compensated by using long propagation lengths.[179, 180] On the other hand, in resonant structures such as metasurfaces one needs to use optical modes with high Q-factor.

So far, the EO effect has been investigated theoretically and experimentally in either one-dimensional[36, 37] or two-dimensional[38, 183] metasurfaces. All these realizations are based on $LiNbO_3$ thin films where the modulating electric field produced by two planar electrodes lies in the metasurface plane and exploits the r_{33} element, which is the largest. In Ref. 36, the EO effect is used to vary the resonant wavelength of a high Q-factor mode (< 10^3) resulting from a quasi-BIC mode formed in a $LiNbO_3$ high-contrast grating (see Figure 7a). While the amplitude variation is small, the phase modulation at a constant wavelength is monitored in an interferometric experiment that demonstrates the dynamic behavior of the structure at a modulation frequency of 1 MHz and a peak-to-peak voltage of 300 V (see Figure 7b). A different approach was followed in Ref. 37, where an unstructured thin film of $LiNbO_3$ supports silicon nanoresonators (see Figure 7c). The variation of the refractive index of the $LiNbO_3$ substrate modifies the field radiated over

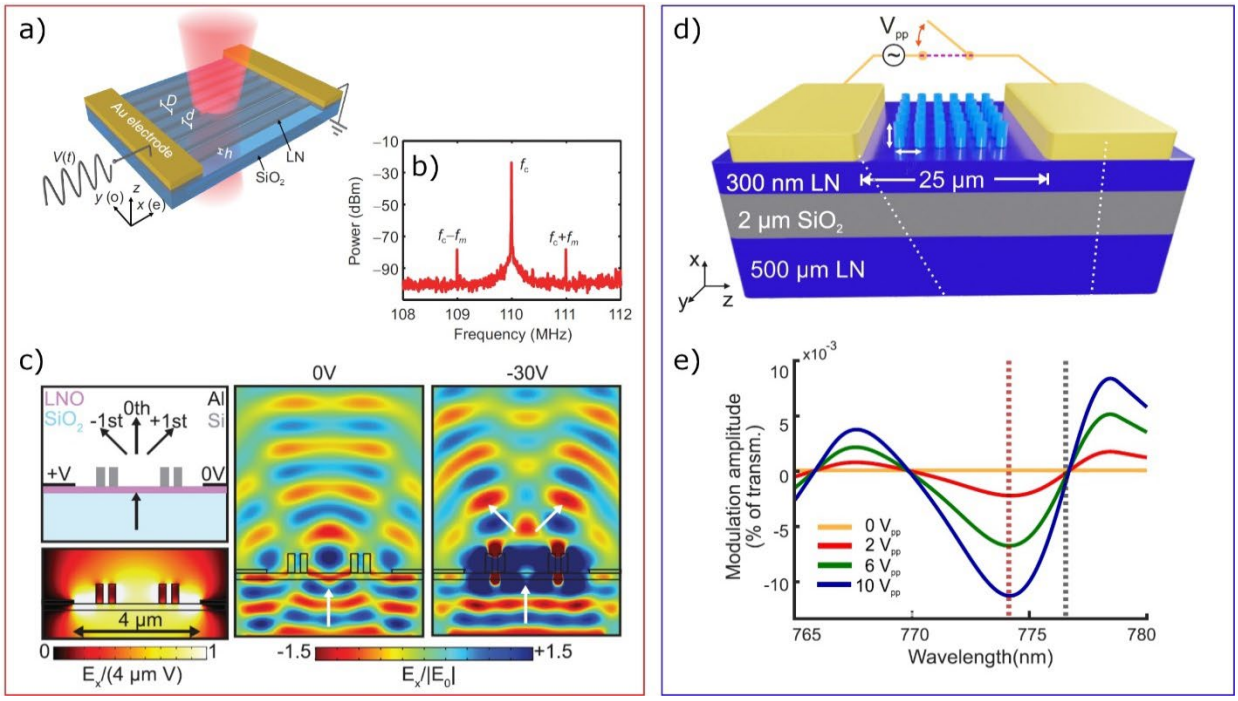

Figure 7. (a) $LiNbO_3$ (LN) on silica grating with Au electrodes sustaining a quasi-bound state in the continuum. (b) Power spectrum of optical beats featuring a carrier frequency of f_c =110 MHz and sidebands at $f_c \pm f_m$ where f_m=1 MHz is the modulation frequency. Panels a,b are reprinted with permission from Ref. 36 © 2021 Springer Nature. (c) High Q-factor beam-splitting device. Top left: schematic of the device. Bottom left: simulated DC electric field distribution when 1 V is applied to the left contact, keeping the right one grounded. Middle: device operating at 1397 nm with no applied voltage. Right: Same device with –30 V voltage. Reproduced with permission from Ref. 37 © 2021 The Authors. (d) Metasurface (light blue LN pillars, dark blue LN bulk layer) between two Au electrodes on top of a silica layer (grey). (e) Dependence of the modulation amplitude on the peak-to-peak AC voltage between 0 and 10 V_{pp} (V_{pp} = 1 V) with 180 kHz driving frequency. Panels d,e are reprinted with permission from Ref. 38 © 2021 American Chemical Society.

the diffraction orders of the structures. High Q-factor modes (> 10^4) were designed and arranged in a device to realize electrically tunable beam-splitting with an applied voltage of 30 V. More recently, a 2D monolithic array of nanodisks was obtained by partial etch of a 500 nm-thick $LiNbO_3$ film and employed to demonstrate fast EO modulation of the linear transmittivity (see Figure 7d).[38] In this structure, a weak refractive-index modulation of the substrate (~10^{-5}) resulted in an amplitude modulation of 0.01% up to 2.5 MHz for peak-to-peak voltages below 1 V (see Figure 7e). The detectable yet small modulation is associated with the limited Q-factor (~10^2) attained in 2D arrangements and to the applied electric field lines that are mainly confined to the unstructured $LiNbO_3$ substrate with limited spatial overlap with the

optical electric field of the resonance. In Ref. 183 the resonant frequency of a plasmonic metasurface on a thin $LiNbO_3$ film was modulated. In contrast to the previously mentioned works, the modulating radio-frequency field lines are transverse to the metasurface plane, resulting in a small separation between the electrodes, which does not depend on the metasurface area. By applying a peak-to-peak voltage of 24 V, the reflectance was modulated by 40% with a modulation bandwidth of almost 800 kHz.

Reference	Q-factor	Dimension (μm^2)	V_{pp} (V)	Modulation rate (MHz)	Wavelength (nm)
B.F. Gao et al. [36]	$<10^3$	10 × 10	300	1	633
D. Barton et al. [37] (only numerical)	2.8×10^4	4 μm, not specified in the other dimension	30	N.A.	1397
H. Weigand et al. [38]	129	20 × 20	10	2.5	774.2
A.Weiss, et al. [183]	70	130 × 130	24	0.8	1535

Table 4. Selected measurements and simulations of EO modulation by $LiNbO_3$ metasurfaces.

Thanks to its successful applications in integrated photonics, $LiNbO_3$ appears to be the natural choice to realize metasurface-based EO devices. However, alternative ferroelectric materials, such as barium titanate ($BaTiO_3$) may compete with the $LiNbO_3$ platform, thanks to their larger Pockels coefficients. With respect to $LiNbO_3$, $BaTiO_3$ is often grown in polycrystalline form, which randomizes the nonlinear optical response and increases the complexity of modeling, design, and fabrication.[84] Yet, very recently it was shown that crystalline $BaTiO_3$ thin films can be grown on both silicon[53] as well as low index isolating substrates.[184, 185] Such platforms are extremely promising for EO applications since they demonstrated extremely large Pockels coefficients, with r_{33} values up to 340 pm/V,[53] that is, one order of magnitude higher than in $LiNbO_3$. The challenges of top-down nanofabrication listed in detail in Section 3, along with the advancements in bottom-up nanofabrication, fostered the investigation of metasurfaces composed of $BaTiO_3$ nanoparticle films for EO applications.[52, 85] However, sizable drops in the values of the Pockels coefficient as well as the $\chi^{(2)}$ have been reported for nanoparticles of small size (*e.g.* r_{33}~37 pm/V for 50 nm nanoparticle diameter).[84, 85] Other materials, like organic polymers, can also show large EO coefficients.[186]

Recently, EO silicon metasurfaces were realized by infiltrating them with JRD1:PMMA that exhibits r_{33}~100 pm/V.[187] Despite such large Pockels coefficients, organic polymers are typically affected by temperature and chemical instabilities. Finally, strained silicon was also suggested as an innovative route to attain a large Pockels effect.[188, 189] Whether these material alternatives would be able to replace $LiNbO_3$ for optical metasurfaces remains to be seen.

4.3.2. Perspective applications of electro-optic metasurfaces

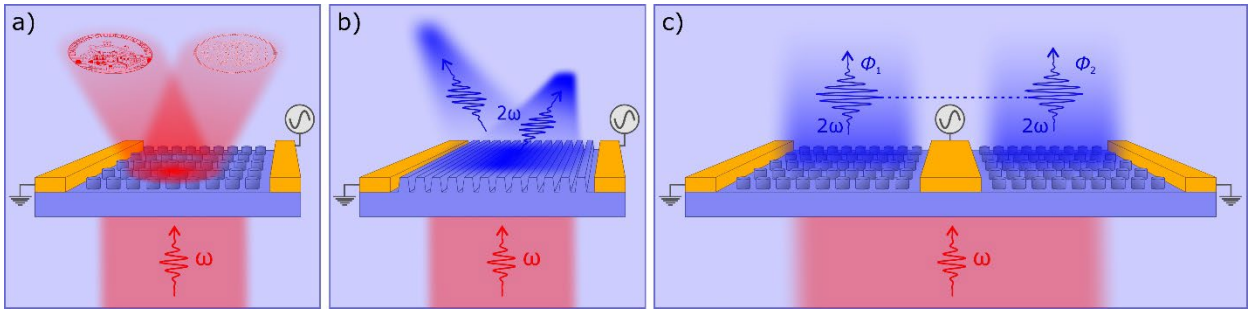

Figure 8. Potential applications of electro-optic control with $LiNbO_3$ metasurfaces. (a) Concept of an electro-optically controlled metasurface for optical signal re-routing and generation of polarization states. (b) Concept of an electro-optically controlled 1D metalens for harmonic generation and dynamical steering of the nonlinear emission. (c) Concept of an electro-optically controlled pair of metasurfaces imparting a relative phase difference between the nonlinearly generated wavefronts in view of sensing applications.

The use of EO effects to dynamically control the optical response of $LiNbO_3$ metasurfaces has just began. The first works discussed above highlight the critical challenge of enhancing the local electric field to sensibly exploit the small change of refractive index induced by the Pockels effect. Therefore, future developing trends might focus on engineering the spatial profiles of the high Q-factor optical modes to increase the overlap with the applied electric field inside the metasurface volume. From a fabrication perspective, the capability to place the electrical contacts on the top and the bottom of sub-micrometer thin resonators will likely boost the modulation strength and reduce the operating voltage.

Harnessing the EO effect in $LiNbO_3$ nanostructures and metasurfaces may pave the way for a new generation of fast compact devices for free-space optical communications, including LiFi technologies. Indeed, new concepts aimed at improving the modulation depth and the temporal response of the EO

phenomenon will stimulate the development of a novel class of free-space spatial light modulators for fast on-demand generation of light states[187] and re-routing of optical signals as depicted in Figure 8a. To achieve these goals, it will be essential to address the voltage drop across each pixel of the metasurface with high efficiency and short response time. In the framework of reconfigurable light wavefront, another interesting application of EO metasurfaces is the realization of linear and nonlinear smart lenses, *e.g.*, where the focal distance of the lens can be changed dynamically by local control of the phase response as a function of the applied voltage (see Figure 8b). Other functionalities that can be enabled by the EO control over the light wavefront is the active control of the beam directionality and the transverse location of the focus (see Figure 8b). This is an appealing application that can lead to the development of fast-scanning focused beams. The dynamic control of the polarization state of the output beam will be utterly interesting, as many applications rely on the polarization state of light.

Finally, a dynamic control of the phase of the transmitted light enables the realization of miniaturized interferometers (see Figure 8c). For example, an incident beam could illuminate two identical metasurfaces. If one metasurface response is modulated via the EO effect, the relative phase difference (or phase delay $\varphi_2 - \varphi_1$) between the two transmitted beams could be controlled. Such a system will provide an extremely compact, highly precise and ultra-stable control of the relative delay in comparison to mechanical systems. Electro-optically modulated metasurfaces might be used also as image sensors. For example, in Ref. 190 an area is patterned with several gratings with different periodicities. The presence of an object between the grating and a receiver can be reconstructed by analyzing the modulation frequencies at the detector. Another interesting prospective application field stems from the possibility to control the material permittivity with fast (few GHz) modulation rates.[191] Indeed, this feature entails the possibility to realize magnetic-free nonreciprocal optical devices such as isolators and circulators that are essential building blocks in many applications.

5. Conclusions

In conclusion, the field of $LiNbO_3$-based nonlinear and tunable meta-optics has lately received great research attention driven by recent advances in nanofabrication. In this perspective, we provide a viewpoint on the potential applications of $LiNbO_3$-based metasurfaces for light conversion, management, and quantum optics. At the same time, we have critically appraised the possible setbacks and limitations of the $LiNbO_3$ platform. $LiNbO_3$ is endowed with several undoubtable advantages with respect to other materials, the most notable ones being its broad transparency range in combination with its multifunctionality. Nonetheless, some applications might potentially suffer from its relatively low refractive index, which would limit the field confinement, hence potentially reducing the nonlinear optical and electro-optical performances of $LiNbO_3$-based meta-optics compared to other dielectric platforms. Yet, the recent demonstrations of nonlinear light conversion, photon-pair generation, and electro-optical modulation in ultra-flat monolithic $LiNbO_3$ metasurfaces set such platforms among the most promising tools for light manipulation at the nanoscale, especially in the spectral range from the visible to the MIR. We are confident that these successful endeavors will trigger further investigations and further improvements of $LiNbO_3$ nanofabrication. These will pave the way to the realization of high Q-factor metasurfaces, which might be the breakthrough needed for translating $LiNbO_3$-based meta-optics towards real-world technological applications.

References

[1] H.-T. Chen, A. J. Taylor and N. Yu, "A Review of Metasurfaces: Physics and Applications," *Rep. Prog. Phys.,* vol. 79, p. 076401, 2016.

[2] P. Genevet, F. Capasso, F. Aieta, M. Khorasaninejad and R. Devlin, "Recent Advances in Planar Optics: From Plasmonic to Dielectric Metasurfaces," *Optica,* vol. 4, p. 139–152, 2017.

[3] P. Lalanne and P. Chavel, "Metalenses at Visible Wavelengths: Past, Present, Perspectives," *Laser Photonics Rev.,* vol. 11, p. 1600295, 2017.

[4] F. Capasso, "The Future and Promise of Flat Optics: A Personal Perspective," *Nanophotonics,* vol. 7, p. 953–957, 2018.

[5] O. Quevedo-Teruel, H. Chen, A. Díaz-Rubio, G. Gok, A. Grbic, G. Minatti, E. Martini, S. Maci, G. V. Eleftheriades, M. Chen, N. I. Zheludev, N. Papasimakis, S. Choudhury, Z. A. Kudyshev, S. Saha, H. Reddy, A. Boltasseva, V. M. Shalaev, A. V. Kildishev, D. Sievenpiper, C. Caloz, A. Alù, Q. He, L. Zhou, G. Valerio, E. Rajo-Iglesias, Z. Sipus, F. Mesa, R. Rodríguez-Berral, F. Medina, V. Asadchy, S. Tretyakov and C. Craeye, "Roadmap on Metasurfaces," *J. Opt.,* vol. 21, p. 073002, 2019.

[6] W. T. Chen, A. Y. Zhu and F. Capasso, "Flat Optics with Dispersion-Engineered Metasurfaces," *Nat. Rev. Mater.,* vol. 5, p. 604–620, 2020.

[7] J. Scheuer, "Optical Metasurfaces Are Coming of Age: Short- and Long-term Opportunities for Commercial Applications," *ACS Photonics,* vol. 7, p. 1323–1354, 2020.

[8] M. Piccardo, V. Ginis, A. Forbes, S. Mahler, A. A. Friesem, N. Davidson, H. Ren, A. H. Dorrah, F. Capasso, F. T. Dullo, B. S. Ahluwalia, A. Ambrosio, S. Gigan, N. Treps, M. Hiekkamäki, R. Fickler, M. Kues, D. Moss, R. Morandotti, J. Riemensberger, T. J. Kippenberg, J. Faist, G. Scalari, N. Picqué, T. W. Hänsch, G. Cerullo, C. Manzoni, L. A. Lugiato, M. Brambilla, L. Columbo, A. Gatti, F. Prati, A. Shiri, A. F. Abouraddy, A. Alù, E. Galiffi, J. B. Pendry and P. A. Huidobro, "Roadmap on Multimode Light Shaping," *J. Opt.,* vol. 24, p. 013001, 2021.

[9] D. Neshev and I. Aharonovich, "Optical Metasurfaces: New Generation Building Blocks for Multi-Functional Optics," *Light Sci. Appl.,* vol. 7, p. 58, 2018.

[10] C. Wang, Z. Li, M.-H. Kim, X. Xiong, X.-F. Ren, G.-C. Guo, N. Yu and M. Lončar, "Metasurface-Assisted Phase-Matching-Free Second Harmonic Generation in Lithium Niobate Waveguides," *Nat. Commun.,* vol. 8, p. 2098, 2017.

[11] G. Li, S. Zhang and T. Zentgraf, "Nonlinear Photonic Metasurfaces," *Nat. Rev. Mater.,* vol. 2, p. 1–14, 2017.

[12] Y. Zhao, Y. Yang and H.-B. Sun, "Nonlinear Meta-Optics Towards Applications," *PhotoniX,* vol. 2, p. 3, 2021.

[13] G. Grinblat, "Nonlinear Dielectric Nanoantennas and Metasurfaces: Frequency Conversion and Wavefront Control," *ACS Photonics,* vol. 8, p. 3406–3432, 2021.

[14] R. Boyd, Nonlinear Optics, Academic Press, 2008.

[15] C. Trovatello, A. Marini, X. Xu, C. Lee, F. Liu, N. Curreli, C. Manzoni, S. Dal Conte, K. Yao, A. Ciattoni, J. Hone, X. Zhu, P. J. Schuck and G. Cerullo, "Optical Parametric Amplification by Monolayer Transition Metal Dichalcogenides," *Nat. Photonics,* vol. 15, p. 6–10, 2021.

[16] E. Rahimi and R. Gordon, "Nonlinear Plasmonic Metasurfaces," *Adv. Opt. Mater.,* vol. 6, p. 1800274, 2018.

[17] M. Rahmani, G. Leo, I. Brener, A. V. Zayats, S. A. Maier, C. De Angelis, H. Tan, V. F. Gili, F. Karouta, R. Oulton, K. Vora, M. Lysevych, I. Staude, L. Xu, A. E. Miroshnichenko, C. Jagadish and D. N. Neshev, "Nonlinear Frequency Conversion in Optical Nanoantennas and Metasurfaces: Materials Evolution and Fabrication," *Opto-Electron. Adv.,* vol. 1, p. 18002101, 2018.

[18] T. Pertsch and Y. Kivshar, "Nonlinear Optics with Resonant Metasurfaces," *MRS Bull.,* vol. 45, p. 210–220, 2020.

[19] C. De Angelis, G. Leo and D. N. Neshev, Eds., Nonlinear Meta-Optics, CRC Press, 2020.

[20] M. R. Shcherbakov, D. N. Neshev, B. Hopkins, A. S. Shorokhov, I. Staude, E. V. Melik-Gaykazyan, M. Decker, A. A. Ezhov, A. E. Miroshnichenko, I. Brener, A. A. Fedyanin and Y. S. Kivshar, "Enhanced Third-Harmonic Generation in Silicon Nanoparticles Driven by Magnetic Response," *Nano Lett.,* vol. 14, p. 6488–6492, 2014.

[21] L. Wang, S. Kruk, K. Koshelev, I. Kravchenko, B. Luther-Davies and Y. Kivshar, "Nonlinear Wavefront Control with All-Dielectric Metasurfaces," *Nano Lett.,* vol. 18, p. 3978–3984, 2018.

[22] B. Reineke, B. Sain, R. Zhao, L. Carletti, B. Liu, L. Huang, C. De Angelis and T. Zentgraf, "Silicon Metasurfaces for Third Harmonic Geometric Phase Manipulation and Multiplexed Holography," *Nano Lett.,* vol. 19, p. 6585–6591, 2019.

[23] V. F. Gili, L. Carletti, A. Locatelli, D. Rocco, M. Finazzi, L. Ghirardini, I. Favero, C. Gomez, A. Lemaître, M. Celebrano, C. De Angelis and G. Leo, "Monolithic AlGaAs Second-Harmonic Nanoantennas," *Opt. Express,* vol. 24, p. 15965–15971, 2016.

[24] S. Liu, M. B. Sinclair, S. Saravi, G. A. Keeler, Y. Yang, J. Reno, G. M. Peake, F. Setzpfandt, I. Staude, T. Pertsch and I. Brener, "Resonantly Enhanced Second-Harmonic Generation Using III–V Semiconductor All-Dielectric Metasurfaces," *Nano Lett.,* vol. 16, p. 5426–5432, 2016.

[25] F. J. F. Löchner, A. N. Fedotova, S. Liu, G. A. Keeler, G. M. Peake, S. Saravi, M. R. Shcherbakov, S. Burger, A. A. Fedyanin, I. Brener, T. Pertsch, F. Setzpfandt and I. Staude, "Polarization-Dependent Second Harmonic Diffraction from Resonant GaAs Metasurfaces," *ACS Photonics,* vol. 5, p. 1786–1793, 2018.

[26] G. Marino, C. Gigli, D. Rocco, A. Lemaître, I. Favero, C. De Angelis and G. Leo, "Zero-Order Second Harmonic Generation from AlGaAs-on-Insulator Metasurfaces," *ACS Photonics,* vol. 6, p. 1226–1231, 2019.

[27] S. Saravi, T. Pertsch and F. Setzpfandt, "Lithium Niobate on Insulator: An Emerging Platform for Integrated Quantum Photonics," *Adv. Opt. Mater.,* vol. 9, p. 2100789, 2021.

[28] D. Zhu, L. Shao, M. Yu, R. Cheng, B. Desiatov, C. J. Xin, Y. Hu, J. Holzgrafe, S. Ghosh, A. Shams-Ansari, E. Puma, N. Sinclair, C. Reimer, M. Zhang and M. Lončar, "Integrated Photonics on Thin-Film Lithium Niobate," *Adv. Opt. Photon.,* vol. 13, p. 242–352, 2021.

[29] A. Honardoost, K. Abdelsalam and S. Fathpour, "Rejuvenating a Versatile Photonic Material: Thin-Film Lithium Niobate," *Laser Photonics Rev.,* vol. 14, p. 2000088, 2020.

[30] L. Carletti, C. Li, J. Sautter, I. Staude, C. De Angelis, T. Li and D. N. Neshev, "Second Harmonic Generation in Monolithic Lithium Niobate Metasurfaces," *Opt. Express,* vol. 27, p. 33391–33398, 2019.

[31] Z. Huang, M. Wang, Y. Li, J. Shang, K. Li, W. Qiu, J. Dong, H. Guan, Z. Chen and H. Lu, "Highly Efficient Second Harmonic Generation of Thin Film Lithium Niobate Nanograting near Bound States in the Continuum," *Nanotechnology,* vol. 32, p. 325207, 2021.

[32] B. Gao, M. Ren, W. Wu, H. Hu, W. Cai and J. Xu, "Lithium Niobate Metasurfaces," *Laser Photonics Rev.,* vol. 13, p. 1800312, 2019.

[33] A. Fedotova, M. Younesi, J. Sautter, A. Vaskin, F. J. F. Löchner, M. Steinert, R. Geiss, T. Pertsch, I. Staude and F. Setzpfandt, "Second-Harmonic Generation in Resonant Nonlinear Metasurfaces Based on Lithium Niobate," *Nano Lett.,* vol. 20, p. 8608–8614, 2020.

[34] L. Carletti, A. Zilli, F. Moia, A. Toma, M. Finazzi, C. De Angelis, D. N. Neshev and M. Celebrano, "Steering and Encoding the Polarization of the Second Harmonic in the Visible with a Monolithic $LiNbO_3$ Metasurface," *ACS Photonics,* vol. 8, p. 731–737, 2021.

[35] J. Ma, F. Xie, W. Chen, J. Chen, W. Wu, W. Liu, Y. Chen, W. Cai, M. Ren and J. Xu, "Nonlinear Lithium Niobate Metasurfaces for Second Harmonic Generation," *Laser Photonics Rev.,* vol. 15, p. 2000521, 2021.

[36] B. Gao, M. Ren, W. Wu, W. Cai and J. Xu, "Electro-Optic Lithium Niobate Metasurfaces," *Sci. China Phys. Mech. Astron.,* vol. 64, p. 240362, 2021.

[37] D. Barton, M. Lawrence and J. Dionne, "Wavefront Shaping and Modulation with Resonant Electro-Optic Phase Gradient Metasurfaces," *Appl. Phys. Lett.,* vol. 118, p. 071104, 2021.

[38] H. Weigand, V. V. Vogler-Neuling, M. Reig Escalé, D. Pohl, F. U. Richter, A. Karvounis, F. Timpu and R. Grange, "Enhanced Electro-Optic Modulation in Resonant Metasurfaces of Lithium Niobate," *ACS Photonics,* vol. 8, p. 3004–3009, 2021.

[39] D. A. Roberts, "Simplified Characterization of Uniaxial and Biaxial Nonlinear Optical Crystals: A Plea for Standardization of Nomenclature and Conventions," *IEEE J. Quantum Electron.,* vol. 28, p. 2057–2074, 1992.

[40] I. Shoji, T. Kondo, A. Kitamoto, M. Shirane and R. Ito, "Absolute Scale of Second-Order Nonlinear-Optical Coefficients," *J. Opt. Soc. Am. B,* vol. 14, p. 2268–2294, 1997.

[41] T. Santiago-Cruz, A. Fedotova, V. Sultanov, M. A. Weissflog, D. Arslan, M. Younesi, T. Pertsch, I. Staude, F. Setzpfandt and M. Chekhova, "Photon Pairs from Resonant Metasurfaces," *Nano Lett.,* vol. 21, p. 4423–4429, 2021.

[42] J. Zhang, J. Ma, M. Parry, M. Cai, R. Camacho-Morales, L. Xu, D. N. Neshev and A. A. Sukhorukov, "Spatially Entangled Photon Pairs from Lithium Niobate Nonlocal Metasurfaces," *Sci. Adv.,* vol. 8, eabq4240, 2022.

[43] R. Schiek and T. Pertsch, "Absolute Measurement of the Quadratic Nonlinear Susceptibility of Lithium Niobate in Waveguides," *Opt. Mater. Express,* vol. 2, p. 126–139, 2012.

[44] E. H. Turner, "High-Frequency Electro-Optic Coefficients of Lithium Niobate," *Appl. Phys. Lett.,* vol. 8, p. 303–304, 1966.

[45] I. P. Kaminow and W. D. Johnston, "Quantitative Determination of Sources of the Electro-Optic Effect in $LiNbO_3$ and $LiTaO_3$," *Phys. Rev.,* vol. 160, p. 519–522, 1967.

[46] I. Shoji, T. Kondo and R. Ito, "Second-Order Nonlinear Susceptibilities of Various Dielectric and Semiconductor Materials," *Opt. Quant. Electron.,* vol. 34, p. 797–833, 2002.

[47] C.-A. Berseth, C. Wuethrich and F. K. Reinhart, "The Electro-Optic Coefficients of GaAs: Measurements at 1.32 and 1.5 μm and Study of Their Dispersion between 0.9 and 10 μm," *J. Appl. Phys.,* vol. 71, p. 2821–2825, 1992.

[48] D. F. Nelson and E. H. Turner, "Electro-Optic and Piezoelectric Coefficients and Refractive Index of Gallium Phosphide," *J. Appl. Phys.,* vol. 39, p. 3337–3343, 1968.

[49] N. A. Sanford, A. V. Davydov, D. V. Tsvetkov, A. V. Dmitriev, S. Keller, U. K. Mishra, S. P. DenBaars, S. S. Park, J. Y. Han and R. J. Molnar, "Measurement of Second Order Susceptibilities of GaN and AlGaN," *J. Appl. Phys.,* vol. 97, p. 053512, 2005.

[50] X.-C. Long, R. A. Myers, S. R. J. Brueck, R. Ramer, K. Zheng and S. D. Hersee, "GaN Linear Electro-Optic Effect," *Appl. Phys. Lett.,* vol. 67, p. 1349–1351, 1995.

[51] M. J. Weber, Handbook of Optical Materials, CRC Press, 2018.

[52] A. Karvounis, F. Timpu, V. V. Vogler-Neuling, R. Savo and R. Grange, "Barium Titanate Nanostructures and Thin Films for Photonics," *Adv. Opt. Mater.,* vol. 8, p. 2001249, 2020.

[53] S. Abel, F. Eltes, J. E. Ortmann, A. Messner, P. Castera, T. Wagner, D. Urbonas, A. Rosa, A. M. Gutierrez, D. Tulli, P. Ma, B. Baeuerle, A. Josten, W. Heni, D. Caimi, L. Czornomaz, A. A. Demkov, J. Leuthold, P. Sanchis and J. Fompeyrine, "Large Pockels Effect in Micro- and Nanostructured Barium Titanate Integrated on Silicon," *Nat. Mater.,* vol. 18, p. 42–47, 2018.

[54] W. Song, G.-Y. Guo, S. Huang, L. Yang and L. Yang, "First-Principles Studies of Second-Order Nonlinear Optical Properties of Organic-Inorganic Hybrid Halide Perovskites," *Phys. Rev. Appl.,* vol. 13, p. 014052, 2020.

[55] Y. Gao, G. Walters, Y. Qin, B. Chen, Y. Min, A. Seifitokaldani, B. Sun, P. Todorovic, M. I. Saidaminov, A. Lough, S. Tongay, S. Hoogland and E. H. Sargent, "Electro-Optic Modulation in Hybrid Metal Halide Perovskites," *Adv. Mater.,* vol. 31, p. 1808336, 2019.

[56] A. J. Mercante, S. Shi, P. Yao, L. Xie, R. M. Weikle and D. W. Prather, "Thin Film Lithium Niobate Electro-Optic Modulator with Terahertz Operating Bandwidth," *Opt. Express,* vol. 26, p. 14810–14816, 2018.

[57] V. V. Vogler-Neuling, A. Karvounis, A. Morandi, H. Weigand, E. Dénervaud and R. Grange, "Photonic Assemblies of Randomly Oriented Nanocrystals for Engineered Nonlinear and Electro-Optic Effects," *ACS Photonics,* vol. 9, p. 2193–2203, 2022.

[58] R. S. Weis and T. K. Gaylord, "Lithium Niobate: Summary of Physical Properties and Crystal Structure," *Appl. Phys. A,* vol. 37, p. 191–203, 1985.

[59] G. Poberaj, M. Koechlin, F. Sulser, A. Guarino, J. Hajfler and P. Günter, "Ion-Sliced Lithium Niobate Thin Films for Active Photonic Devices," *Opt. Mater.,* vol. 31, p. 1054–1058, 2009.

[60] G. Poberaj, H. Hu, W. Sohler and P. Guenter, "Lithium Niobate on Insulator (LNOI) for Micro-Photonic Devices," *Laser Photonics Rev.,* vol. 6, p. 488–503, 2012.

[61] J. Lin, F. Bo, Y. Cheng and J. Xu, "Advances in On-Chip Photonic Devices Based on Lithium Niobate on Insulator," *Photon. Res.,* vol. 8, p. 1910–1936, 2020.

[62] F. Laurell, J. Webjorn, G. Arvidsson and J. Holmberg, "Wet Etching of Proton-Exchanged Lithium Niobate – A Novel Processing Technique," *J. Lightwave Technol.,* vol. 10, p. 1606–1609, 1992.

[63] F. Chen, X.-L. Wang and K.-M. Wang, "Development of Ion-Implanted Optical Waveguides in Optical Materials: A Review," *Opt. Mater.,* vol. 29, p. 1523–1542, 2007.

[64] J. Thomas, M. Heinrich, P. Zeil, V. Hilbert, K. Rademaker, R. Riedel, S. Ringleb, C. Dubs, J.-P. Ruske, S. Nolte and A. Tünnermann, "Laser Direct Writing: Enabling Monolithic and Hybrid Integrated Solutions on the Lithium Niobate Platform," *Phys. Status Solidi A,* vol. 208, p. 276–283, 2011.

[65] J. Lin, Y. Xu, Z. Fang, M. Wang, J. Song, N. Wang, L. Qiao, W. Fang and Y. Cheng, "Fabrication of High-Q Lithium Niobate Microresonators Using Femtosecond Laser Micromachining," *Sci. Rep.,* vol. 5, p. 8072, 2015.

[66] N. Courjal, B. Guichardaz, G. Ulliac, J.-Y. Rauch, B. Sadani, H.-H. Lu and M.-P. Bernal, "High Aspect Ratio Lithium Niobate Ridge Waveguides Fabricated by Optical Grade Dicing," *J. Phys. D,* vol. 44, p. 305101, 2011.

[67] G. Griffiths and R. Esdaile, "Analysis of Titanium Diffused Planar Optical Waveguides in Lithium Niobate," *IEEE J. Quantum Electron.,* vol. 20, p. 149–159, 1984.

[68] F. Lacour, N. Courjal, M.-P. Bernal, A. Sabac, C. Bainier and M. Spajer, "Nanostructuring Lithium Niobate Substrates by Focused Ion Beam Milling," *Opt. Mater.,* vol. 27, p. 1421–1425, 2005.

[69] G. Ulliac, B. Guichardaz, J.-Y. Rauch, S. Queste, S. Benchabane and N. Courjal, "Ultra-Smooth $LiNbO_3$ Micro and Nano Structures for Photonic Applications," *Microelectron. Eng.,* vol. 88, p. 2417–2419, 2011.

[70] B. Fang, H. Li, S. Zhu and T. Li, "Second-Harmonic Generation and Manipulation in Lithium Niobate Slab Waveguides by Grating Metasurfaces," *Photonics Res.,* vol. 8, p. 1296–1300, 2020.

[71] G. Si, A. J. Danner, S. L. Teo, E. J. Teo, J. Teng and A. A. Bettiol, "Photonic Crystal Structures with Ultrahigh Aspect Ratio in Lithium Niobate Fabricated by Focused Ion Beam Milling," *J. Vac. Sci. Technol. A,* vol. 29, p. 021205, 2011.

[72] G. Ulliac, V. Calero, A. Ndao, F. I. Baida and M.-P. Bernal, "Argon Plasma Inductively Coupled Plasma Reactive Ion Etching Study for Smooth Sidewall Thin Film Lithium Niobate Waveguide Application," *Opt. Mater.,* vol. 53, p. 1–5, 2016.

[73] Z. Liu, Y. Xu, Y. Lin, J. Xiang, T. Feng, Q. Cao, J. Li, S. Lan and J. Liu, "High-Q Quasibound States in the Continuum for Nonlinear Metasurfaces," *Phys. Rev. Lett.,* vol. 123, p. 253901, 2019.

[74] S. Yuan, Y. Wu, Z. Dang, C. Zeng, X. Qi, G. Guo, X. Ren and J. Xia, "Strongly Enhanced Second Harmonic Generation in a Thin Film Lithium Niobate Heterostructure Cavity," *Phys. Rev. Lett.,* vol. 127, p. 153901, 2021.

[75] F. Timpu, J. Sendra, C. Renaut, L. Lang, M. Timofeeva, M. T. Buscaglia, V. Buscaglia and R. Grange, "Lithium Niobate Nanocubes as Linear and Nonlinear Ultraviolet Mie Resonators," *ACS Photonics,* vol. 6, p. 545–552, 2019.

[76] J. Wang, Z. Liu, J. Xiang, B. Chen, Y. Wei, W. Liu, Y. Xu, S. Lan and J. Liu, "Ultraviolet Second Harmonic Generation from Mie-Resonant Lithium Niobate Nanospheres," *Nanophotonics,* vol. 10, p. 4273–4278, 2021.

[77] R. Savo, A. Morandi, J. S. Müller, F. Kaufmann, F. Timpu, M. Reig Escalé, M. Zanini, L. Isa and R. Grange, "Broadband Mie Driven Random Quasi-Phase-Matching," *Nat. Photonics,* vol. 14, p. 740–747, 2020.

[78] R. Faryad Ali and B. D. Gates, "Lithium Niobate Particles with a Tunable Diameter and Porosity for Optical Second Harmonic Generation," *RSC Advances,* vol. 12, p. 822–833, 2022.

[79] A. R. Kamali and D. J. Fray, "Preparation of Lithium Niobate Particles Via Reactive Molten Salt Synthesis Method," *Ceram. Int.,* vol. 40, p. 1835–1841, 2014.

[80] Y. Wang, X. Y. Zhou, Z. Chen, B. Cai, Z. Z. Ye, C. Y. Gao and J. Y. Huang, "Synthesis of Cubic $LiNbO_3$ Nanoparticles and Their Application in Vitro Bioimaging," *Appl. Phys. A,* vol. 117, p. 2121–2126, 2014.

[81] B. D. Wood, V. Mocanu and B. D. Gates, "Solution-Phase Synthesis of Crystalline Lithium Niobate Nanostructures," *Adv. Mater.,* vol. 20, p. 4552–4556, 2008.

[82] D. Mohanty, G. S. Chaubey, A. Yourdkhani, S. Adireddy, G. Caruntu and J. B. Wiley, "Synthesis and Piezoelectric Response of Cubic and Spherical $LiNbO_3$ Nanocrystals," *RSC Adv.,* vol. 2, p. 1913–1916, 2012.

[83] R. F. Ali and B. D. Gates, "Synthesis of Lithium Niobate Nanocrystals with Size Focusing through an Ostwald Ripening Process," *Chem. Mater.,* vol. 30, p. 2028–2035, 2018.

[84] E. Kim, A. Steinbrück, M. T. Buscaglia, V. Buscaglia, T. Pertsch and R. Grange, "Second-harmonic Generation of Single $BaTiO_3$ Nanoparticles down to 22 nm Diameter," *ACS Nano,* vol. 7, p. 5343–5349, 2013.

[85] A. Karvounis, V. V. Vogler-Neuling, F. U. Richter, E. Dénervaud, M. Timofeeva and R. Grange, "Electro-Optic Metasurfaces Based on Barium Titanate Nanoparticle Films," *Adv. Opt. Mater.,* vol. 8, p. 2000623, 2020.

[86] C. Rendón-Barraza, F. Timpu, R. Grange and S. Brasselet, "Crystalline Heterogeneity in Single Ferroelectric Nanocrystals Revealed by Polarized Nonlinear Microscopy," *Sci. Rep.,* vol. 9, p. 1670, 2019.

[87] Y. Shiratori, C. Pithan, J. Dornseiffer and R. Waser, "Raman Scattering Studies on Nanocrystalline $BaTiO_3$ Part II – Consolidated Polycrystalline Ceramics," *J. Raman Spectrosc.,* vol. 38, p. 1300–1306, 2007.

[88] L. Vittadello, M. Imlau, F. Alarslan, J. Klein, Q. A. Khan, M. Haase, H. Schäfer and M. Steinhart, "Rapid Patterning of Nonlinear Optical 2D-Photonic Crystals on Indium Tin Oxide," in *Conference on Lasers and Electro-Optics*, paper AM4I.4, 2022.

[89] S. Aghaeimeibodi, B. Desiatov, J.-H. Kim, C.-M. Lee, M. A. Buyukkaya, A. Karasahin, C. J. K. Richardson, R. P. Leavitt, M. Lončar and E. Waks, "Integration of Quantum Dots with Lithium Niobate Photonics," *Appl. Phys. Lett.,* vol. 113, p. 221102, 2018.

[90] S. Dutta, E. A. Goldschmidt, S. Barik, U. Saha and E. Waks, "Integrated Photonic Platform for Rare-Earth Ions in Thin Film Lithium Niobate," *Nano Lett.,* vol. 20, p. 741–747, 2019.

[91] X. Jiang, D. Pak, A. Nandi, Y. Xuan and M. Hosseini, "Rare Earth-Implanted Lithium Niobate: Properties and On-Chip Integration," *Appl. Phys. Lett.,* vol. 115, p. 071104, 2019.

[92] O. Sánchez-Dena, S. D. Villalobos-Mendoza, R. Farías and C. D. Fierro-Ruiz, "Lithium Niobate Single Crystals and Powders Reviewed—Part II," *Crystals,* vol. 10, p. 990, 2020.

[93] B. M. Jin, I. W. Kim, W. B. White and A. S. Bhalla, "Modification of UV–VIS Optical Absorption Properties Caused by MgO Incorporation in MgO-Doped $LiNbO_3$ Crystals," *Mater. Lett.,* vol. 30, p. 385–388, 1997.

[94] U. Schlarb, M. Wöhlecke, B. Gather, A. Reichert, K. Betzler, T. Volk and N. Rubinina, "Refractive Indices of Zn-Doped Lithium Niobate," *Opt. Mater.,* vol. 4, p. 791–795, 1995.

[95] Y. Yang, D. Psaltis, M. Luennemann, D. Berben, U. Hartwig and K. Buse, "Photorefractive Properties of Lithium Niobate Crystals Doped with Manganese," *J. Opt. Soc. Am. B,* vol. 20, p. 1491–1502, 2003.

[96] O. Beyer, I. Breunig, F. Kalkum and K. Buse, "Photorefractive Effect in Iron-Doped Lithium Niobate Crystals Induced by Femtosecond Pulses of 1.5 μm Wavelength," *Appl. Phys. Lett.,* vol. 88, p. 051120, 2006.

[97] V. M. N. Passaro and F. Magno, "Holographic Gratings in Photorefractive Materials: A Review," *Laser Phys.,* vol. 17, p. 231–243, 2007.

[98] Y. Kong, F. Bo, W. Wang, D. Zheng, H. Liu, G. Zhang, R. Rupp and J. Xu, "Recent Progress in Lithium Niobate: Optical Damage, Defect Simulation, and On-Chip Devices," *Adv. Mater.,* vol. 32, p. 1806452, 2019.

[99] Z. Wang, Z. Fang, Z. Liu, W. Chu, Y. Zhou, J. Zhang, R. Wu, M. Wang, T. Lu and Y. Cheng, "On-Chip Tunable Microdisk Laser Fabricated on Er^{3+}-Doped Lithium Niobate on Insulator," *Opt. Lett.,* vol. 46, p. 380–383, 2021.

[100] Q. Luo, Z. Hao, C. Yang, R. Zhang, D. Zheng, S. Liu, H. Liu, F. Bo, Y. Kong, G. Zhang and J. Xu, "Microdisk Lasers on an Erbium-Doped Lithium-Niobite Chip," *Sci. China Phys. Mech. Astron.,* vol. 64, p. 234263, 2021.

[101] Z. Chen, Q. Xu, K. Zhang, W.-H. Wong, D.-L. Zhang, E. Y.-B. Pun and C. Wang, "Efficient Erbium-Doped Thin-Film Lithium Niobate Waveguide Amplifiers," *Opt. Lett.,* vol. 46, p. 1161–1164, 2021.

[102] J. Zhou, Y. Liang, Z. Liu, W. Chu, H. Zhang, D. Yin, Z. Fang, R. Wu, J. Zhang, W. Chen, Z. Wang, Y. Zhou, M. Wang and Y. Cheng, "On-Chip Integrated Waveguide Amplifiers on Erbium-Doped Thin-Film Lithium Niobate on Insulator," *Laser Photonics Rev.,* vol. 15, p. 2100030, 2021.

[103] Q. Luo, C. Yang, Z. Hao, R. Zhang, R. Ma, D. Zheng, H. Liu, X. Yu, F. Gao, F. Bo, Y. Kong, G. Zhang and J. Xu, "On-Chip Ytterbium-Doped Lithium Niobate Microdisk Lasers with High Conversion Efficiency," *Opt. Lett.,* vol. 47, p. 854–857, 2022.

[104] V. Y. Shur, A. R. Akhmatkhanov and I. S. Baturin, "Micro- and Nano-Domain Engineering in Lithium Niobate," *Appl. Phys. Rev.,* vol. 2, p. 040604, 2015.

[105] X. Wu, L. Zhang, Z. Hao, R. Zhang, R. Ma, F. Bo, G. Zhang and J. Xu, "Broadband Second-Harmonic Generation in Step-Chirped Periodically Poled Lithium Niobate Waveguides," *Opt. Lett,* vol. 47, p. 1574–1577, 2022.

[106] M. Jankowski, C. Langrock, B. Desiatov, A. Marandi, C. Wang, M. Zhang, C. R. Phillips, M. Lončar and M. M. Fejer, "Ultrabroadband Nonlinear Optics in Nanophotonic Periodically Poled Lithium Niobate Waveguides," *Optica,* vol. 7, p. 40–46, 2020.

[107] B. Mu, X. Wu, Y. Niu, Y. Chen, X. Cai, Y. Gong, Z. Xie, X. Hu and S. Zhu, "Locally Periodically Poled LNOI Ridge Waveguide for Second Harmonic Generation," *Chin. Opt. Lett.,* vol. 19, p. 060007, 2021.

[108] J. Zhao, M. Rüsing, M. Roeper, L. M. Eng and S. Mookherjea, "Poling Thin-Film x-Cut Lithium Niobate for Quasi-Phase Matching with Sub-Micrometer Periodicity," *J. Appl. Phys.,* vol. 127, p. 193104, 2020.

[109] E. O. Vlasov, D. S. Chezganov, L. V. Gimadeeva, E. A. Pashnina, E. D. Greshnyakov, M. A. Chuvakova and V. Y. Shur, "E-Beam Domain Patterning in Thin Plates of MgO-Doped $LiNbO_3$," *Ferroelectrics,* vol. 542, p. 85–92, 2019.

[110] G. Rosenman, P. Urenski, A. Agronin, Y. Rosenwaks and M. Molotskii, "Submicron Ferroelectric Domain Structures Tailored by High-voltage Scanning Probe Microscopy," *Appl. Phys. Lett.,* vol. 82, p. 103–105, 2003.

[111] J. T. Nagy and R. M. Reano, "Submicrometer Periodic Poling of Lithium Niobate Thin Films with Bipolar Preconditioning Pulses," *Opt. Mater. Express,* vol. 10, p. 1911–1920, 2020.

[112] M. Younesi, R. Geiss, S. Rajaee, F. Setzpfandt, Y.-H. Chen and T. Pertsch, "Periodic Poling with a Micrometer-Range Period in Thin-Film Lithium Niobate on Insulator," *J. Opt. Soc. Am. B,* vol. 38, p. 685–691, 2021.

[113] B. N. Slautin, H. Zhu and V. Y. Shur, "Submicron Periodical Poling in Z-Cut Lithium Niobate Thin Films," *Ferroelectrics,* vol. 576, p. 119–128, 2021.

[114] A. Fedotova, M. Younesi, D. Arslan, T. Pertsch, I. Staude and F. Setzpfandt, "Second-Harmonic Generation from Metasurfaces with Spatially Engineered Nonlinearity," in *Conference on Lasers and Electro-Optics*, paper FTh4B.7, 2022.

[115] C. Gigli, T. Wu, G. Marino, A. Borne, G. Leo and P. Lalanne, "Quasinormal-Mode Non-Hermitian Modeling and Design in Nonlinear Nano-Optics," *ACS Photonics,* vol. 7, p. 1197–1205, 3 April 2020.

[116] M. Celebrano, X. Wu, M. Baselli, S. Großmann, P. Biagioni, A. Locatelli, C. De Angelis, G. Cerullo, R. Osellame, B. Hecht, L. Duò, F. Ciccacci and M. Finazzi, "Mode Matching in Multiresonant Plasmonic Nanoantennas for Enhanced Second Harmonic Generation," *Nat. Nanotechnol.,* vol. 10, p. 412–417, 2015.

[117] Z. Lin, X. Liang, M. Lončar, S. G. Johnson and A. W. Rodriguez, "Cavity-Enhanced Second-Harmonic Generation Via Nonlinear-Overlap Optimization," *Optica,* vol. 3, p. 233–238, 2016.

[118] A. Sergeyev, R. Geiss, A. S. Solntsev, A. A. Sukhorukov, F. Schrempel, T. Pertsch and R. Grange, "Enhancing Guided Second-Harmonic Light in Lithium Niobate Nanowires," *ACS Photonics,* vol. 2, p. 687–691, 2015.

[119] R. Geiss, S. Saravi, A. Sergeyev, S. Diziain, F. Setzpfandt, F. Schrempel, R. Grange, E.-B. Kley, A. Tünnermann and T. Pertsch, "Fabrication of Nanoscale Lithium Niobate Waveguides for Second-Harmonic Generation," *Opt. Lett.,* vol. 40, p. 2715–2718, 2015.

[120] Y. Li, Z. Huang, Z. Sui, H. Chen, X. Zhang, W. Huang, H. Guan, W. Qiu, J. Dong, W. Zhu, J. Yu, H. Lu and Z. Chen, "Optical Anapole Mode in Nanostructured Lithium Niobate for Enhancing Second Harmonic Generation," *Nanophotonics,* vol. 9, p. 3575–3585, 2020.

[121] D. Lehr, J. Reinhold, I. Thiele, H. Hartung, K. Dietrich, C. Menzel, T. Pertsch, E.-B. Kley and A. Tünnermann, "Enhancing Second Harmonic Generation in Gold Nanoring Resonators Filled with Lithium Niobate," *Nano Lett.,* vol. 15, p. 1025–1030, 2015.

[122] Q.-S. Liu, B. Cheng, M.-H. Chao, W.-J. Zhang, Y. Xu and G.-F. Song, "Giant Nonlinear Circular Dichroism from High Q-Factor Asymmetric Lithium Niobate Metasurfaces," *Ann. Phys.,* vol. 533, p. 2100255, 2021.

[123] L. Kang, H. Bao and D. H. Werner, "Efficient Second-Harmonic Generation in High Q-Factor Asymmetric Lithium Niobate Metasurfaces," *Opt. Lett.,* vol. 46, p. 633–636, 2021.

[124] K.-H. Kim, "Low-Index Dielectric Metasurfaces Supported by Metallic Substrates for Efficient Second-Harmonic Generation in the Blue-ultraviolet Range," *Phys. Chem. Chem. Phys.,* vol. 22, p. 7300–7305, 2020.

[125] C. Wang, M. J. Burek, Z. Lin, H. A. Atikian, V. Venkataraman, I.-C. Huang, P. Stark and M. Lončar, "Integrated High Quality Factor Lithium Niobate Microdisk Resonators," *Opt. Express,* vol. 22, p. 30924–30933, 2014.

[126] M. Li, H. Liang, R. Luo, Y. He and Q. Lin, "High-Q 2D Lithium Niobate Photonic Crystal Slab Nanoresonators," *Laser Photonics Rev.,* vol. 13, p. 1800228, 2019.

[127] C. W. Hsu, B. Zhen, A. D. Stone, J. D. Joannopoulos and M. Soljačić, "Bound States in the Continuum," *Nat. Rev. Mater.,* vol. 1, p. 16048, 2016.

[128] X. Zhang, L. He, X. Gan, X. Huang, Y. Du, Z. Zhai, Z. Li, Y. Zheng, X. Chen, Y. Cai and X. Ao, "Quasi-Bound States in the Continuum Enhanced Second-Harmonic Generation in Thin-Film Lithium Niobate," *Laser Photonics Rev.,* vol. 16, p. 2200031, 2022.

[129] J. J. R. Yepes, F. I. Baida and A. Ndao, “Giant Second-Harmonic Generation Enabled by Bound-State Continuum Cavity on Lithium Niobate Membrane,” *arXiv*, 2022-06-22, 2206.11405v1 (accessed 2022-10-05).

[130] Q. Yang, Y. Liu, X. Gan, C. Fang, G. Han and Y. Hao, "Nonlinear Bound States in the Continuum of Etchless Lithium Niobate Metasurfaces," *IEEE Photonics J.,* vol. 12, p. 1–9, 2020.

[131] M. Esseling, A. Zaltron, C. Sada and C. Denz, "Charge Sensor and Particle Trap Based on z-Cut Lithium Niobate," *Appl. Phys. Lett.,* vol. 103, p. 061115, 2013.

[132] A. Zaltron, G. Bettella, G. Pozza, R. Zamboni, M. Ciampolillo, N. Argiolas, C. Sada, S. Kroesen, M. Esseling and C. Denz, "Integrated Optics on Lithium Niobate for Sensing Applications," *Proc. SPIE Vol. 9506, Optical Sensors 2015*, 950608, 2015.

[133] G. Bettella, R. Zamboni, G. Pozza, A. Zaltron, C. Montevecchi, M. Pierno, G. Mistura, C. Sada, L. Gauthier-Manuel and M. Chauvet, "$LiNbO_3$ Integrated System for Opto-Microfluidic Sensing," *Sens. Actuators B Chem.,* vol. 282, p. 391–398, 2019.

[134] J. Rollinson, M. Hella, S. Toroghi, P. Rabiei and I. Wilke, "Thin-film Lithium Niobate Modulators for Non-Invasive Sensing of High-frequency Electric Fields," *J. Opt. Soc. Am. B,* vol. 38, p. 336–341, 2021.

[135] C. Schlickriede, N. Waterman, B. Reineke, P. Georgi, G. Li, S. Zhang and T. Zentgraf, "Imaging through Nonlinear Metalens Using Second Harmonic Generation," *Adv. Mater.,* vol. 30, p. 1703843, 2018.

[136] R. Camacho-Morales, D. Rocco, L. Xu, V. F. Gili, N. Dimitrov, L. Stoyanov, Z. Ma, A. Komar, M. Lysevych, F. Karouta, A. A. Dreischuh, H. H. H. Tan, G. Leo, C. De Angelis, C. Jagadish, A. E. Miroshnichenko, M. Rahmani and D. N. Neshev, "Infrared Upconversion Imaging in Nonlinear Metasurfaces," *Adv. Photonics,* vol. 3, p. 036002, 2021.

[137] A. Zilli, D. Rocco, M. Finazzi, A. Di Francescantonio, L. Duò, C. Gigli, G. Marino, G. Leo, C. De Angelis and M. Celebrano, "Frequency Tripling via Sum-Frequency Generation at the Nanoscale," *ACS Photonics,* vol. 8, p. 1175–1182, 2021.

[138] C. Schlickriede, S. S. Kruk, L. Wang, B. Sain, Y. Kivshar and T. Zentgraf, "Nonlinear Imaging with All-Dielectric Metasurfaces," *Nano Lett.,* vol. 20, p. 4370–4376, 2020.

[139] J. D. Caldwell, L. Lindsay, V. Giannini, I. Vurgaftman, T. L. Reinecke, S. A. Maier and O. J. Glembocki, "Low-loss, Infrared and Terahertz Nanophotonics Using Surface Phonon Polaritons," *Nanophotonics,* vol. 4, p. 44–68, 2015.

[140] S. Foteinopoulou, G. C. R. Devarapu, G. S. Subramania, S. Krishna and D. Wasserman, "Phonon-Polaritonics: Enabling Powerful Capabilities for Infrared Photonics," *Nanophotonics,* vol. 8, p. 2129–2175, 2019.

[141] K. Murate and K. Kawase, "Perspective: Terahertz Wave Parametric Generator and Its Applications," *J. Appl. Phys.,* vol. 124, p. 160901, 2018.

[142] Y. Lu, Q. Zhang, Q. Wu, Z. Chen, X. Liu and J. Xu, "Giant Enhancement of THz-Frequency Optical Nonlinearity by Phonon Polariton in Ionic Crystals," *Nat. Commun.,* vol. 12, p. 3183, 2021.

[143] A. Herter, A. Shams-Ansari, F. F. Settembrini, H. K. Warner, J. Faist, M. Lončar and I.-C. Benea-Chelmus, "Terahertz Waveform Synthesis from Integrated Lithium Niobate Circuits," *arXiv*, 2022-04-25, 2204.11725v1 (accessed 2022-10-05).

[144] E. M. Kleist and M. T. Ruggiero, "Advances in Low-Frequency Vibrational Spectroscopy and Applications in Crystal Engineering," *Cryst. Growth Des.,* vol. 22, p. 939–953, 2022.

[145] T. R. Globus, D. L. Woolard, T. Khromova, T. W. Crowe, M. Bykhovskaia, B. L. Gelmont, J. Hesler and A. C. Samuels, "THz-Spectroscopy of Biological Molecules," *J. Biol. Phys.,* vol. 29, p. 89–100, 2003.

[146] R. J. Falconer and A. G. Markelz, "Terahertz Spectroscopic Analysis of Peptides and Proteins," *J. Infrared Millim. Terahertz Waves,* vol. 33, p. 973–988, 2012.

[147] P. H. Siegel, "Terahertz Technology in Biology and Medicine," *IEEE Trans. Microw. Theory Techn.,* vol. 52, p. 2438–2447, 2004.

[148] Y. Roh, S.-H. Lee, J. Kwak, H. S. Song, S. Shin, Y. K. Kim, J. W. Wu, B.-K. Ju, B. Kang and M. Seo, "Terahertz Imaging with Metamaterials for Biological Applications," *Sens. Actuators B Chem.,* vol. 352, p. 130993, 2022.

[149] J. F. Federici, B. Schulkin, F. Huang, D. Gary, R. Barat, F. Oliveira and D. Zimdars, "THz Imaging and Sensing for Security Applications—Explosives, Weapons and Drugs," *Semicond. Sci. Tech.,* vol. 20, p. S266–S280, 2005.

[150] L. Hu, B. Wang, Y. Guo, S. Du, J. Chen, J. Li, C. Gu and L. Wang, "Quasi-BIC Enhanced Broadband Terahertz Generation in All-Dielectric Metasurface," *Adv. Opt. Mater.,* vol. 10, p. 2200193, 2022.

[151] Q. Guo, R. Sekine, L. Ledezma, R. Nehra, D. J. Dean, A. Roy, R. M. Gray, S. Jahani and A. Marandi, "Femtojoule Femtosecond All-Optical Switching in Lithium Niobate Nanophotonics," *Nat. Photonics,* vol. 16, p. 625–631, 2022.

[152] C. Zhang, Y.-F. Huang, B.-H. Liu, C.-F. Li and G.-C. Guo, "Spontaneous Parametric Down-Conversion Sources for Multiphoton Experiments," *Adv. Quantum Technol.,* vol. 4, p. 2000132, 2021.

[153] C. Okoth, A. Cavanna, T. Santiago-Cruz and M. V. Chekhova, "Microscale Generation of Entangled Photons without Momentum Conservation," *Phys. Rev. Lett.,* vol. 123, p. 263602, 2019.

[154] C. Okoth, E. Kovlakov, F. Bönsel, A. Cavanna, S. Straupe, S. P. Kulik and M. V. Chekhova, "Idealized Einstein–Podolsky–Rosen States from Non–Phase-Matched Parametric Down-Conversion," *Phys. Rev. A,* vol. 101, p. 011801, 2020.

[155] T. Santiago-Cruz, V. Sultanov, H. Zhang, L. A. Krivitsky and M. V. Chekhova, "Entangled Photons from Subwavelength Nonlinear Films," *Opt. Lett.,* vol. 46, p. 653–656, 2021.

[156] K. Wang, M. Chekhova and Y. Kivshar, "Metasurfaces for Quantum Technologies," *Phys. Today,* vol. 75, p. 38–44, 2022.

[157] A. S. Solntsev, G. S. Agarwal and Y. S. Kivshar, "Metasurfaces for Quantum Photonics," *Nat. Photonics,* vol. 15, p. 327–336, 2021.

[158] W. J. M. Kort-Kamp, A. K. Azad and D. A. R. Dalvit, "Space-Time Quantum Metasurfaces," *Phys. Rev. Lett.,* vol. 127, p. 043603, 2021.

[159] L. Li, Z. Liu, X. Ren, S. Wang, V.-C. Su, M.-K. Chen, C. H. Chu, H. Y. Kuo, B. Liu, W. Zang, G. Guo, L. Zhang, Z. Wang, S. Zhu and D. P. Tsai, "Metalens-Array–Based High-Dimensional and Multiphoton Quantum Source," *Science,* vol. 368, p. 1487–1490, 2020.

[160] M. Parry, A. Mazzanti, A. N. Poddubny, G. Della Valle, D. N. Neshev and A. A. Sukhorukov, "Enhanced Generation of Nondegenerate Photon Pairs in Nonlinear Metasurfaces," *Adv. Photonics,* vol. 3, p. 055001, 2021.

[161] A. Mazzanti, M. Parry, A. N.Poddubny, G. Della Valle, D. N. Neshev and A. A. Sukhorukov, "Enhanced Generation of Angle Correlated Photon-Pairs in Nonlinear Metasurfaces," *New J. Phys.,* vol. 24, p. 035006, 2022.

[162] K. Wang, J. G. Titchener, S. S. Kruk, L. Xu, H.-P. Chung, M. Parry, I. I. Kravchenko, Y.-H. Chen, A. S. Solntsev, Y. S. Kivshar, D. N. Neshev and A. A. Sukhorukov, "Quantum Metasurface for Multiphoton Interference and State Reconstruction," *Science,* vol. 361, p. 1104–1108, 2018.

[163] B. Jin, D. Mishra and C. Argyropoulos, "Efficient Single-Photon Pair Generation by Spontaneous Parametric Down-Conversion in Nonlinear Plasmonic Metasurfaces," *Nanoscale,* vol. 13, no. 47, p. 19903–19914, 2021.

[164] N. M. H. Duong, G. Saerens, F. Timpu, M. T. Buscaglia, V. Buscaglia, A. Morandi, J. S. Müller, A. Maeder, F. Kaufmann, A. S. Solntsev and R. Grange, "Spontaneous Parametric Down-Conversion in Bottom-up Grown Lithium Niobate Microcubes," *Opt. Mater. Express,* vol. 12, p. 3696–3704, 2022.

[165] T. Santiago-Cruz, S. D. Gennaro, O. Mitrofanov, S. Addamane, J. Reno, I. Brener and M. V. Chekhova, "Resonant Metasurfaces for Generating Complex Quantum States," *Science,* vol. 377, p. 991–995, 2022.

[166] G. Marino, D. Rocco, C. Gigli, G. Beaudoin, K. Pantzas, S. Suffit, P. Filloux, I. Sagnes, G. Leo and C. De Angelis, "Harmonic Generation with Multi-layer Dielectric Metasurfaces," *Nanophotonics,* vol. 10, p. 1837–1843, 2021.

[167] V. Sultanov, T. Santiago-Cruz and M. V. Chekhova, "Flat-Optics Generation of Broadband Photon Pairs with Tunable Polarization Entanglement," *Opt. Lett.,* vol. 47, p. 3872–3875, 2022.

[168] G. Marino, A. S. Solntsev, L. Xu, V. F. Gili, L. Carletti, A. N. Poddubny, M. Rahmani, D. A. Smirnova, H. Chen, A. Lemaître, G. Zhang, A. V. Zayats, C. De Angelis, G. Leo, A. A. Sukhorukov and D. N. Neshev, "Spontaneous Photon-Pair Generation from a Dielectric Nanoantenna," *Optica,* vol. 6, p. 1416–1422, 2019.

[169] A. N. Poddubny, I. V. Iorsh and A. A. Sukhorukov, "Generation of Photon-Plasmon Quantum States in Nonlinear Hyperbolic Metamaterials," *Phys. Rev. Lett.,* vol. 117, p. 123901, 2016.

[170] A. Nikolaeva, K. Frizyuk, N. Olekhno, A. Solntsev and M. Petrov, "Directional Emission of Down-Converted Photons from a Dielectric Nanoresonator," *Phys. Rev. A,* vol. 103, p. 043703, 2021.

[171] M. A. Weissflog, S. Saravi, C. Gigli, G. Marino, R. Dezert, V. Vinel, A. Borne, G. Leo, T. Pertsch and F. Setzpfandt, "Modelling Photon-Pair Generation in Nanoresonators Using Quasinormal Mode Expansions," in *Front. Opt. + Laser Sci. 2021*, paper FTh6C.5, 2021.

[172] I. Aharonovich, D. Englund and M. Toth, "Solid-State Single-Photon Emitters," *Nat. Photonics,* vol. 10, p. 631–641, 2016.

[173] N. Tomm, A. Javadi, N. O. Antoniadis, D. Najer, M. C. Löbl, A. R. Korsch, R. Schott, S. R. Valentin, A. D. Wieck, A. Ludwig and R. J. Warburton, "A Bright and Fast Source of Coherent Single Photons," *Nat. Nanotechnol.,* vol. 16, p. 399–403, 2021.

[174] M. Toth and I. Aharonovich, "Single Photon Sources in Atomically Thin Materials," *Annu. Rev. Phys. Chem.,* vol. 70, p. 123–142, 2019.

[175] D. White, A. Branny, R. J. Chapman, R. Picard, M. Brotons-Gisbert, A. Boes, A. Peruzzo, C. Bonato and B. D. Gerardot, "Atomically-Thin Quantum Dots Integrated with Lithium Niobate Photonic Chips [invited]," *Opt. Mater. Express,* vol. 9, p. 441–448, 2019.

[176] Y. Wang, K. D. Jöns and Z. Sun, "Integrated Photon-Pair Sources with Nonlinear Optics," *Appl. Phys. Rev.,* vol. 8, p. 011314, 2021.

[177] A. Vega, T. Pertsch, F. Setzpfandt and A. A. Sukhorukov, "Metasurface-Assisted Quantum Ghost Discrimination of Polarization Objects," *Phys. Rev. Appl.,* vol. 16, p. 064032, 2021.

[178] A. Vega, E. A. Santos, J. Fuenzalida, M. G. Basset, T. Pertsch, M. Gräfe, S. Saravi and F. Setzpfandt, "Fundamental Resolution Limit of Quantum Imaging with Undetected Photons," *Phys. Rev. Research,* vol. 4, p. 033252, 2022.

[179] M. Zhang, C. Wang, P. Kharel, D. Zhu and M. Lončar, "Integrated Lithium Niobate Electro-Optic Modulators: When Performance Meets Scalability," *Optica,* vol. 8, p. 652–667, 2021.

[180] C. Wang, M. Zhang, B. Stern, M. Lipson and M. Lončar, "Nanophotonic Lithium Niobate Electro-Optic Modulators," *Opt. Express,* vol. 26, p. 1547–1555, 2018.

[181] L. Carletti, M. Gandolfi, D. Rocco, A. Tognazzi, D. de Ceglia, M. A. Vincenti and C. De Angelis, "Reconfigurable Nonlinear Response of Dielectric and Semiconductor Metasurfaces," *Nanophotonics,* vol. 10, p. 4209–4221, 2021.

[182] M. Luennemann, U. Hartwig, G. Panotopoulos and K. Buse, "Electrooptic Properties of Lithium Niobate Crystals for Extremely High External Electric Fields," *Appl. Phys. B,* vol. 76, p. 403–406, 2003.

[183] A. Weiss, C. Frydendahl, J. Bar-David, R. Zektzer, E. Edrei, J. Engelberg, N. Mazurski, B. Desiatov and U. Levy, "Tunable Metasurface Using Thin-Film Lithium Niobate in the Telecom Regime," *ACS Photonics,* vol. 9, p. 605–612, 2022.

[184] Y. Cao, S. L. Tan, E. J. H. Cheung, S. Y. Siew, C. Li, Y. Liu, C. S. Tang, M. Lal, G. Chen, K. Dogheche, P. Yang, S. Pennycook, A. T. S. Wee, S. Chua, E. Dogheche, T. Venkatesan and A. Danner, "A Barium Titanate-on-Oxide Insulator Optoelectronics Platform," *Adv. Mater.,* vol. 33, p. 2101128, 2021.

[185] Y. Cao, J. D. Ng, H.-L. Lin, J. Shao, L. Qi, S. Y. Siew, E. Dogheche and A. J. Danner, "A Thin Film Barium Titanate-on-Insulator Optoelectronics Platform with Various Photonic Devices," in *Conference on Lasers and Electro-Optics*, paper STu1C.6, 2022.

[186] I. Taghavi, M. Moridsadat, A. Tofini, S. Raza, N. A. F. Jaeger, L. Chrostowski, B. J. Shastri and S. Shekhar, "Polymer Modulators in Silicon Photonics: Review and Projections," *Nanophotonics,* vol. 11, p. 3855–3870, 2022.

[187] I.-C. Benea-Chelmus, S. Mason, M. L. Meretska, D. L. Elder, D. Kazakov, A. Shams-Ansari, L. R. Dalton and F. Capasso, "Gigahertz Free-Space Electro-Optic Modulators Based on Mie Resonances," *Nat. Commun.,* vol. 13, 3170, 2022.

[188] R. S. Jacobsen, K. N. Andersen, P. I. Borel, J. Fage-Pedersen, L. H. Frandsen, O. Hansen, M. Kristensen, A. V. Lavrinenko, G. Moulin, H. Ou, C. Peucheret, B. Zsigri and A. Bjarklev, "Strained Silicon as a New Electro-Optic Material," *Nature,* vol. 441, p. 199–202, 2006.

[189] M. Berciano, G. Marcaud, P. Damas, X. Le Roux, P. Crozat, C. A. Ramos, D. Pérez-Galacho, D. Benedikovic, D. Marris-Morini, E. Cassan and L. Vivien, "Fast Linear Electro-Optic Effect in a Centrosymmetric Semiconductor," *Commun. Phys.,* vol. 1, p. 64, 2018.

[190] I.-C. Benea-Chelmus, M. L. Meretska, D. L. Elder, M. Tamagnone, L. R. Dalton and F. Capasso, "Electro-Optic Spatial Light Modulator from an Engineered Organic Layer," *Nat. Commun.,* vol. 12, 5928, 2021.

[191] S. Fan, Y. Shi and Q. Lin, "Nonreciprocal Photonics without Magneto-optics," *IEEE Antennas Wirel. Propag. Lett.,* vol. 17, p. 1948–1952, 2018.

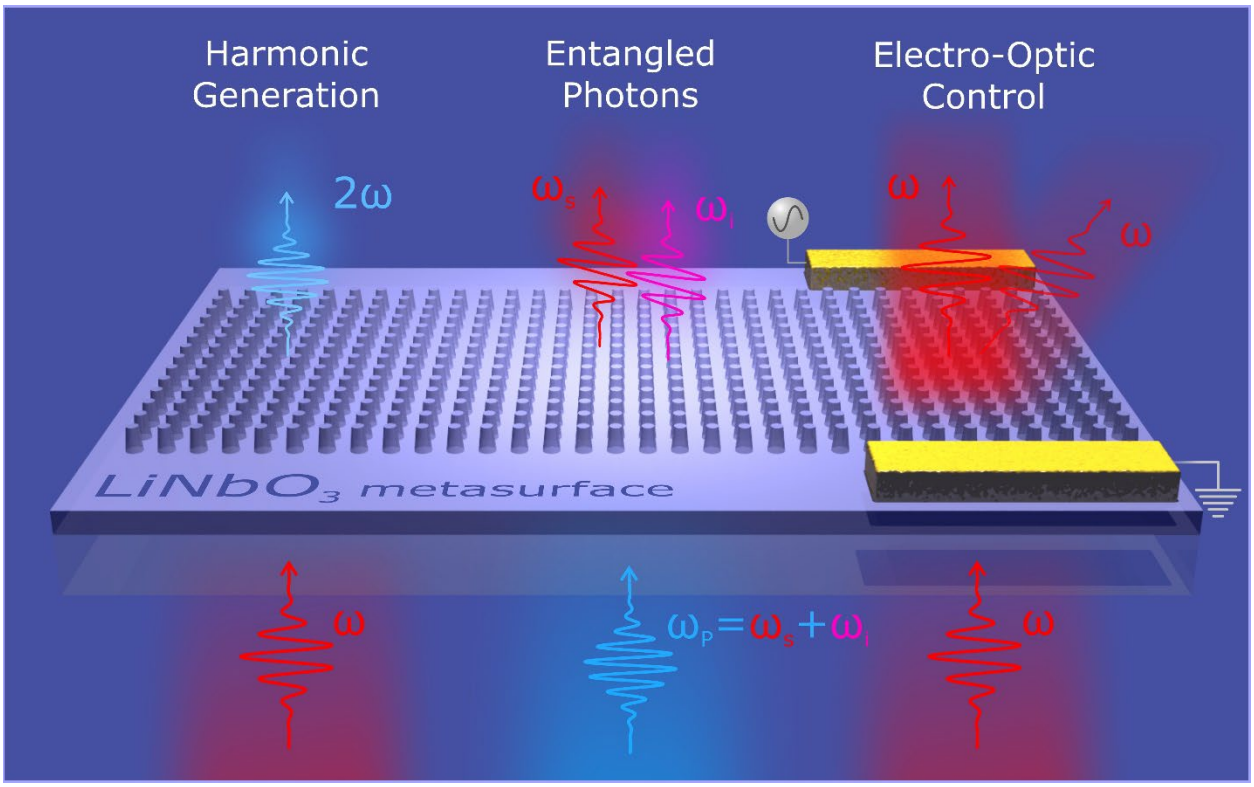

Figure TOC: By engineering $LiNbO_3$-based metasurfaces, one can miniaturize into ultra-thin photonic devices some functionalities of bulk optics such as nonlinear frequency conversion (left), generation of correlated photon pairs (middle) and light steering (right).